SUPPORTING STUDIES IN CLOUD IMAGE PROCESSING FOR PLANETARY FLYBYS OF THE 1970'S

A Semi-Annual Progress Report
on
NASA Grant NGR 50-002-189

for the period
1 January 1976 through 30 June 1976

Verner E. Suomi, Principal Investigator
Robert J. Krauss, Program Manager

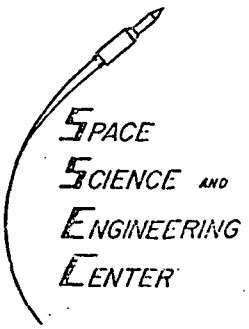

University of Wisconsin-Madison
1225 W. Dayton Street
Madison, Wisconsin 53706

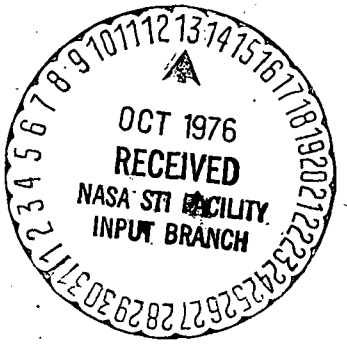

30 August 1976

PROGRAM STATUS

Preparation for the annual meeting of the Division of Planetary Sciences of the American Astronomical Society went smoothly. Two papers were presented on 4 April 1976 dealing with brightness normalization of Mariner 10 Venus images (see last report - Appendix A) and cloud motion measurements (see Appendix A here). In addition, a short 16mm film segment of the cloud motions on Venus was shown, made from McIDAS, our Man-Computer Interactive Data Access System.

Cloud motion measurements have now been extended to three additional data sets covering a period of 12-36 hours following the data previously analyzed last year. The findings are generally in agreement with the previously measured motion field from images taken a day earlier in the flyby mission. There is a small component of meridional motion toward the poles, slightly larger than it was the day earlier. The increase in zonal velocity from equator to mid-latitudes is also still seen.

Two new features were observed in the data. A small amount of eddy transport of momentum toward the poles is present in the measurements. This component is at least one order of magnitude less than the transport by the vortex, so the vortex still appears to be the predominent dynamic feature of the stratospheric motion field on Venus, but the presence of an eddy component increases the possibility of a large global scale wave being present. A second feature just observed in the data is a tendency for zonal velocities at the evening terminator to be smaller than at the subsolar point. This is in conflict with previous observations and we may be observing something new here, as well.

Dennis Phillips returned to SSEC in June and began working on the mosaic navigation of Mariner 10 images again. Dennis spent much of the

winter and spring of 1975-76 on leave from SSEC while he worked on completion of his Ph.D. thesis in applied mathematics. Before he left us, he developed plans to extend the bright limb navigation to the high resolution mosaics of Venus. This is much more complicated, for the least squares fit to the bright limb breaks down if there is insufficient arc length to specify the planet center uniquely. To deal with the mosaics, one must identify both the limb, where it appears, and points of overlap in successive pictures. Then it is necessary to correct for the effect of large scale atmospheric motions during the time interval between the pictures, and iterate to get a best fit for the entire set of frames in the mosaic. When this navigational scheme is operating in late 1976, the first 36 hours worth of Mariner data taken immediately after the Venus encounter will become available to us. This data is extremely crucial for detecting fluctuations in the motion field with periods longer than 2 days. In addition, this new navigation scheme opens up a capability to measure absolute motions of small scale dynamic features.

In Appendix B, Sanjay Limaye has generated a set of adiabatic lapse rate diagrams based on examination of the Venera 8 temperature profile and the Mariner 10 radio occultation data. The motivation for this work was the fact, first mentioned in 1972 by Marov, and since confirmed by several subsequent measurements, that Venus appears to have a slightly superadiabatic lapse rate in the lowest portions of its atmosphere. What this implies is that the whole equatorial region of Venus would have to be in forced convection, a somewhat improbable condition. A deep convective region goes against our Earthlike experience, which says that an atmosphere should be more stratified. Moreover, the Venera and Mariner observations

indicate presence of vertical inhomogeneities and not simply a well mixed atmosphere, as the adiabatic assumption would seem to imply.

Up to now, the lapse rate problem has been virtually ignored. Either the observations are assumed a bit faulty, or else the data reduction is assumed slightly in error because a composition of 100% CO_2 was used. Limaye performs a calculation using the real gas equation and the most accurate available data on CO_2. He reaches the conclusion that a considerably lower concentration of CO_2 must be used in order to explain the vertical lapse rate measurements. Better than 12% nitrogen has to be included to make the measured lapse rate adiabatic. Such a large nitrogen content has not been measured on Venus, so as a result it may be necessary to include dynamic effects or another heavy gas to get all the observations to agree. Observations which have depended on the assumption of 100% CO_2 in their data reduction may be incorrectly interpreted, or at best very naive.

The circulation of a preprint by Mike Belton of Kitt Peak Observatory, containing mercator projections of Mariner 10 pictures of the Venus clouds, has given impetus to the spiral streak line analysis begun here several months ago. The Belton, et.al. pictures show a definite correlation of streak line curvature, latitude position of polar ring, and cloud albedo. Moreover, all of these changes are highly correlated with time variation of our velocity field measurements. A paper on this subject is now being prepared.

ANTICIPATED FUTURE WORK

With seven articles written or in preparation, we have decided to gather them together and issue them in one volume as an institutional publication on the dynamics of the atmosphere of Venus. The papers were recently

submitted to an in-house review, and ought to go into print in October. Two articles written by Suomi and Limaye have been submitted to the Journal of Atmospheric Sciences and should soon pass review.

We have been working to improve the software interfaces in McIDAS to permit faster turnaround between initial image navigation and final data analysis. Many procedures up to now have been one-step-at-a-time sequences where a decision regarding subsequent processing depended on the outcome of a previous step. With the experience we now have, many steps not requiring large computer core space can be automated to improve throughput and turnaround time by almost an order of magnitude. As an example, it took us about 100 weeks to analyze 16 pictures. We anticipate that in the next 16 weeks we should be able to measure an additional 100 pictures and complete all of the large scale wind field analysis from day 38 to day 43 by next spring. In addition, the mosaic navigation being worked on by Dennis Phillips will be operating by September or October. We anticipate several months of shakedown and fine tuning, with some scientific results on small scale motion fields early in 1977.

Sanjay Limaye is working on a Venus remap program which will produce polar stereographic, mercator, or Lambert equal area transforms on McIDAS. This will permit us to examine the Venus image data on McIDAS in a coordinate system which is compatible with the global waves and convection features we are trying to study. This programming work will be completed in early fall. Limaye hopes to have his thesis finished in about 6 months.

We will be experimenting to see if stereo display techniques can be a useful way of presenting, or perhaps even identifying and measuring, small scale dynamic changes in the image data. It is known, for example, that

relative parallax induced in the images by vertical wind shear produces a false stereo effect which separates the motion fields. The low resolution Venus flyby data does not have sufficient image detail to give immediate useful results, although a French observer (Sidi, 1976) was able to use stereo on intermediate resolution data to verify our wind field measurements on day 39. The closeup high resolution mosaic images, with a great deal more image detail, could be very useful in this way.

Work is also going to start soon on application of SMS navigation techniques to Pioneer 10 data from Jupiter. We have programmed McIDAS to read Pioneer tapes. The low level effort in this area has the goals of: a) providing a wind measurement capability for the 1978 Pioneer Venus orbiter, permitting comparisons with Mariner 10 data and enabling long time base studies of the upper atmosphere of Venus; and b) identifying dynamic characteristics of features on Jupiter from Pioneer 10 and 11 images which may influence choice of targets or the type of imaging sequence to be used on the 1979 MJS Jupiter flyby.

Finally, we will be developing plans for a comparative study of dust storms on Earth and Mars. We have recently done some work using SMS data of dust storms in the Sahara in conjunction with Peter Woiceshyn of JPL and we will be archiving similar data in the near future for further study. It turns out that the physics of dust storms on the two planets is quite similar in many respects, and dust storm frequency and genesis is closely correlated with climate changes and food production here on Earth. The dust storm seasons on both Mars and Earth will be approaching in about 6 months. With Viking now in orbit about Mars, this would be an ideal time to initiate a study of dust storms there, and we hope to persuade the Viking

people to look for conditions of dust storm genesis. The archived Viking and SMS data will then serve as a data base for a comparative study, which we will plan when we know how successful the data base acquisition has been.

A proposal will soon be submitted to extend this grant for another year. We anticipate that our Venus wind field study will identify several new characteristics of upper atmosphere motions, and possibly influence the Pioneer Venus Orbiter imaging sequence. Limaye's thesis work, while not definitive concerning the atmospheric dynamic structure, ought to be able to define some observations which may limit our choice of alternative dynamic structures, and possibly he can identify some critical observations which should be made by Pioneer in 1978. This work, plus the other efforts mentioned above, makes the next year perhaps the most significant of all for this grant. Our hard work over the past two years is beginning to pay off.

APPENDIX A

NEW MEASUREMENTS OF UV CLOUD MOTIONS ON VENUS*

Robert Krauss

*Presented at the Division of Planetary Science Meeting of the American Astronomical Society, Austin, Texas, April 4, 1976.

New Measurements of UV Cloud Motions on Venus

Robert J. Krauss

ABSTRACT

Preliminary results of three additional sets of measurements of the velocity of small scale UV cloud features in the Mariner 10 pictures of Venus support findings based on the first measured data set reported by Suomi (1975) and Krauss (1976). The global velocity field consists of a small meridional component towards the poles, increasing linearly with distance from the equator, and a zonal component which is a minimum at the equator and increases toward a maximum near 45° latitude. The differential rotation at low latitudes tends to conserve angular momentum about the poles. Because of the poorer resolution, the solid rotation region above 45° latitude could not be measured in the new data sets. Two new features were observed, however. A small amount of horizontal eddy transport of momentum toward the poles is present in all data sets. In addition, the zonal velocity, zonal velocity gradient with longitude, and the meridional velocity gradient with latitude all show correlated trends suggesting the likelihood of a global velocity field which fluctuates about a mean. However, both the eddy transport and the velocity fluctuations are at least an order of magnitude less than the mean flow. The trend of the zonal velocity gradient indicates that zonal velocities occasionally decelerate toward the evening terminator, throwing doubt on sun-locked mechanisms as drives for the zonal wind.

INTRODUCTION

We present here the preliminary results of additional cloud motion measurements in Mariner 10 UV images of Venus. A previous detailed analysis of four UV images (Krauss, 1976) produced several key observations:

1. The upper atmosphere wind field is organized in a vortex structure with a small meridional flow from equator to poles, and in addition, a zonal flow an order of magnitude greater. The flow pattern causes the atmosphere to rotate differentially at low latitudes (tending to conserve angular momentum about the poles) and to rotate with constant angular velocity at latitudes above 45 degrees, where the atmosphere must converge and sink.

2. The zonal flow accelerates in the sub-solar region. There is a u-component velocity gradient along lines of constant latitude which is about the same size as the v-component velocity gradient along lines of constant longitude. The meridional velocity gradient does not measurably change with latitude.

3. Vertical wind shear is observed in the zonal flow, with higher clouds moving faster. This shear is most likely responsible for a large proportion of measurement scatter visible on the high velocity side of zonal wind profiles.

4. Many kinds of wave phenomena are present in the images, and they complicate analysis of the motion field because waves could carry energy and momentum in addition to that carried by the mass field. The vortex structure in the upper atmosphere appears to be stable and to represent Venus as we usually see it from Earth, but the measured velocity field is likely to be perturbed by several phenomena and thus, at any given time, represents only a single observation and not a mean state of the atmosphere.

In order to better define what the "mean state" is for the Mariner 10 data, we chose to extend the velocity field measurements from the first four pictures (at the start of day 39) into day 40. The main intent was to find out if there were short time variations in the global velocity field. There were really several reasons for picking day 40, however. First, the UV features on Venus show a slight change in character in the period from 2 to 4 days after encounter (closest approach to Venus occurred at $36^{d}\ 17^{h}\ 01^{m}$ GMT). There appears to be an increase in convective activity and generation of brighter clouds near the equator. In addition, the curvature of the spiral streaks increases. A second reason was that if the assumed 4 1/2 day period of the "Y" feature was reflected in the motion field, a time interval of 24-36 hours from the first set of measurements seemed optimal. Too short a time would make changes hard to detect. Too long a time (i.e. 1/2 wavelength or more) would introduce ambiguities in phase. A third reason was that day 40, at ~3 1/2 days past encounter, contained additional interesting features. Both the circumequatorial belts and the bowlike waves were visible. These could be studied in conjunction with the motion field. A fourth consideration was more practical in nature. The 25 km/pixel resolution on day 40 permitted

TABLE I

Data Set Image Identification

DATA SET	FDS NUMBER	GMT DAY	SHUTTER TIME (HHMMSS)GMT
I	62693	39	020656
	62839		034908
	62857		040144
	62987		053244
II	64747	40	020444
	64897		034944
	65023		051756
	65179		070708
III	65343	40	090156
	65473		103256
	65623		121756
	65787		141244
IV	65923	40	154756
	66067		172844
	66223		191756
	66380		210750

TABLE II

ERROR BUDGET ESTIMATE FOR DAY 40

Geometric Rectification	1 pixel
Navigation Model Fit	1½ pixel
Latitude-Longitude Grid	1½ pixel
Roundoff and Truncation	½ pixel
RMS TOTAL	2½ pixel

ERROR BUDGET ESTIMATE FOR DAY 39

Geometric Rectification	1 pixel
Navigation Model Fit	1 pixel
Latitude-Longitude Grid	1 pixel
Roundoff and Truncation	½ pixel
RMS TOTAL	2 pixel

tracking cloud features under 500 km in size. If later images had been used, only larger scale features could have been tracked. Consequently, direct comparison of the velocity profiles with day 39 would have been more subject to question, because the characteristics of the cloud targets used for tracking would have been somewhat different.

Table I identifies the pictures used. The earlier data set from day 39 (Krauss, 1976) is numbered set "I". The data from day 40 is divided into three sets (II, III, and IV) to better identify any trends. In this paper, we report only on preliminary comparison of the COMP or computer measured (cross correlation) velocities from the two days. Single point tracking and target averaging (as for day 39) will be done at a later time.

IMAGE PROCESSING AND ERROR ANALYSIS

The new images in sets II, III, and IV, were processed through the FICOR and GEOM programs at the Jet Propulsion Laboratory and navigated at the University of Wisconsin in exactly the same way as data set I. Extensive error analysis was not repeated, as there seemed no reason to believe that any new sources of error would exist. The previous day's analysis had shown that the true navigation and measurement error was slightly more than half that which was estimated, and had shown that vertical wind shear and changes in cloud shape were the most likely reasons for most of the observed measurement scatter. Without contrary evidence, there was no reason to expect anything different in other data sets, and that indeed appears to be the case here. Except for a larger scatter in the measurements, proportional to the reduced resolution, nothing unusual was seen in the measurements from day 40. Consequently, the present limited analysis appears adequate to determine the trends we seek.

We estimate the limit of useful resolution will probably be reached at 35-40 km/pixel for the velocity measurement techniques used here. At that point, the measurement scatter due to degraded resolution dominates all the structure now visible in the velocity profiles, and one is limited to following only the larger albedo features. Edges and shapes of smaller features are not visible. One can better compare such low resolution measurements with Earth based observations, but the fine structure of the wind field is likely to be lost, and is best observed at resolutions of 10-20 km/pixel, with appropriate time resolution to detect velocity increments of 5 m/s or less.

The wind field measurements are shown in Figures 1, 2, and 3. The order of presentation is: a) data set I - Target averages for 15/15 edit; b) data set I - All data points for day 39; c) data sets II, III, and IV - All data points for day 40; d) data set II alone; e) data set III alone; f) data set IV alone. The data sets for day 40 have fewer cloud targets than day 39 because the lower ground (cloud) resolution made selection and tracking more difficult. Thus, the total of all three data sets is a more reliable indicator of the day's mean velocity field. Note too, the absence of measurements at latitudes above 45° and also the low number of measurements in the northern hemisphere, especially in data set IV. As cloud targets get

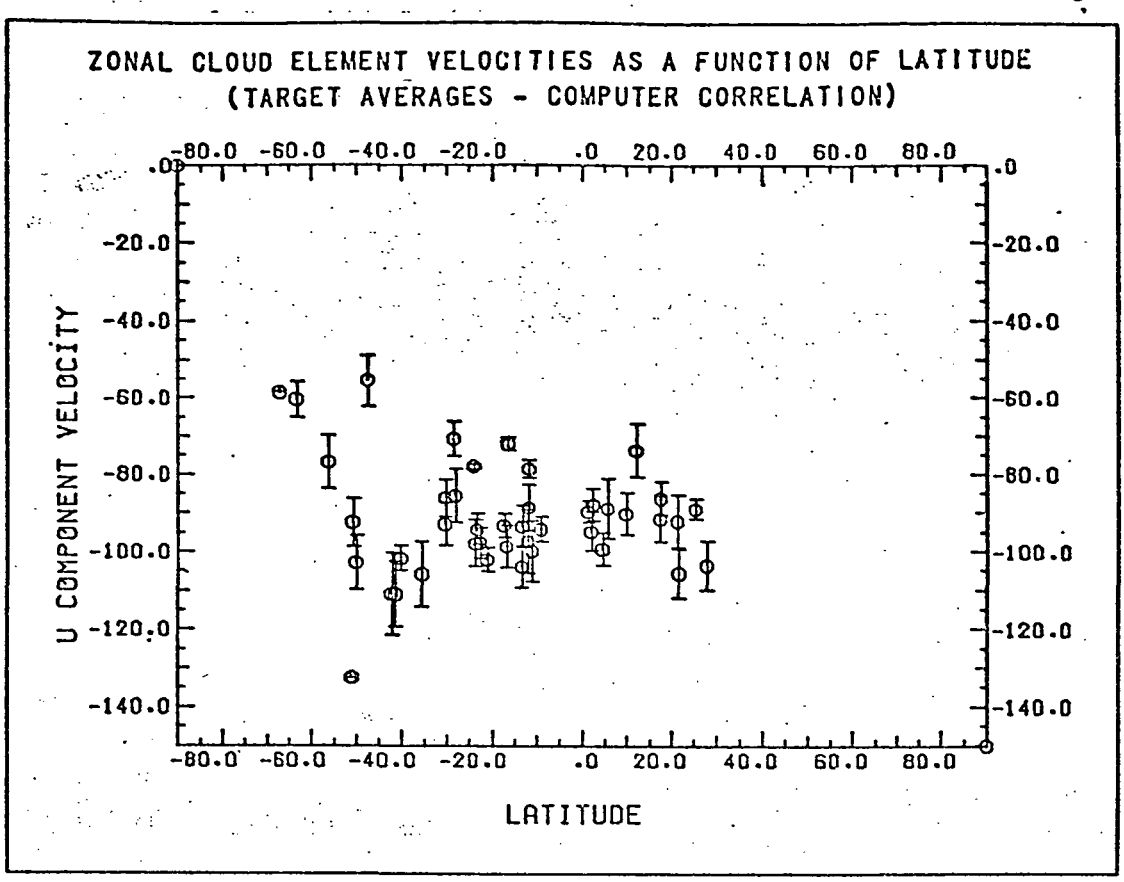

Figure 1a. Target averages for 15 m/s edited measurements -- data set I. The editing and averaging process removes single widely divergent measurements and gives a "cleaner" view of the underlying structure.

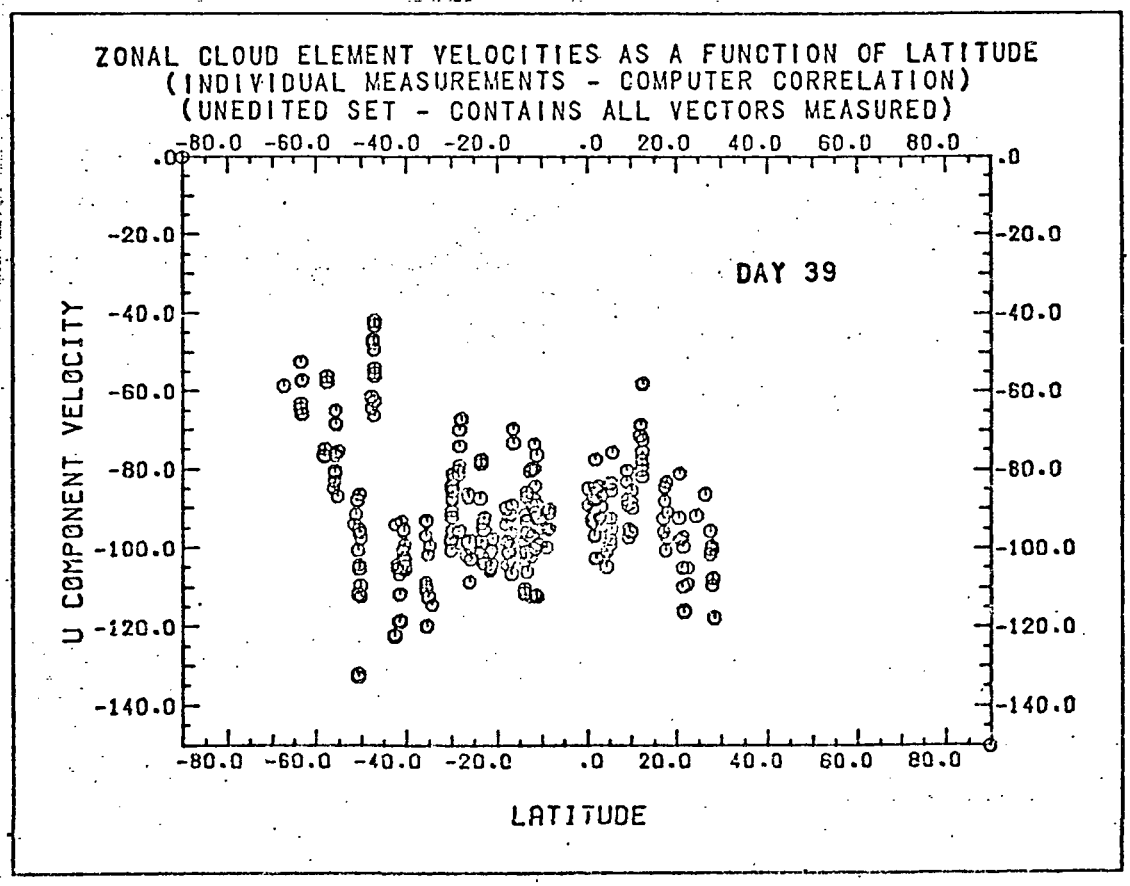

Figure 1b. Unedited measurements for data set I (day 39). Compare with Figures 1 c-f.

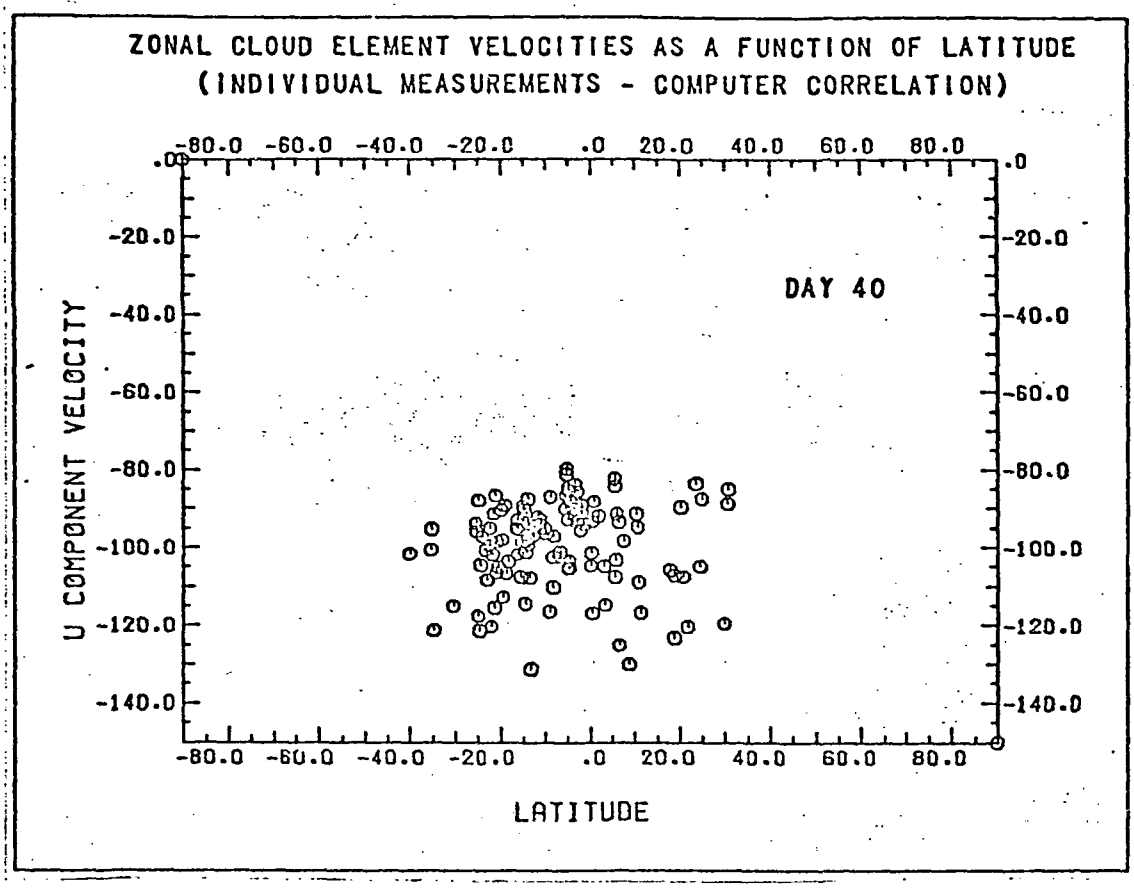

Figure 1c. Unedited measurements for day 40 (sets II, III, and IV, combined).

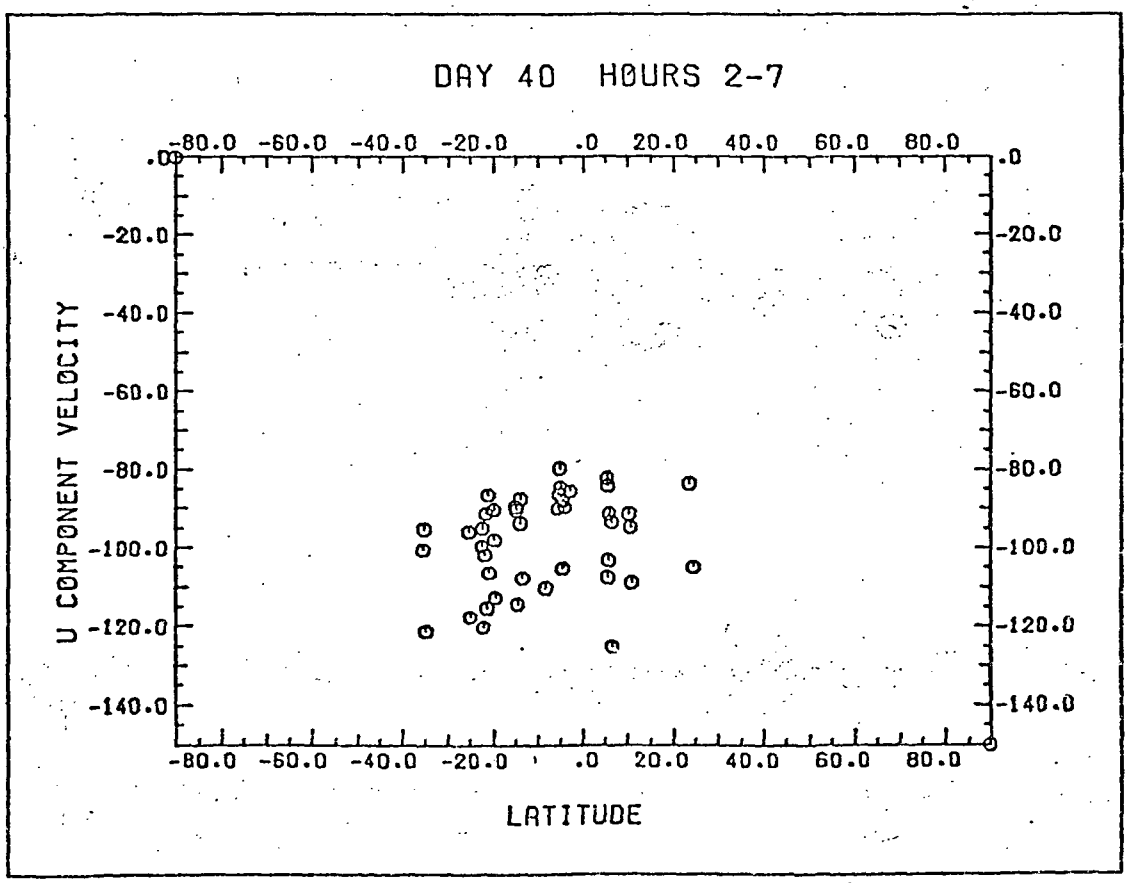

Figure 1d. Unedited measurements for set II.

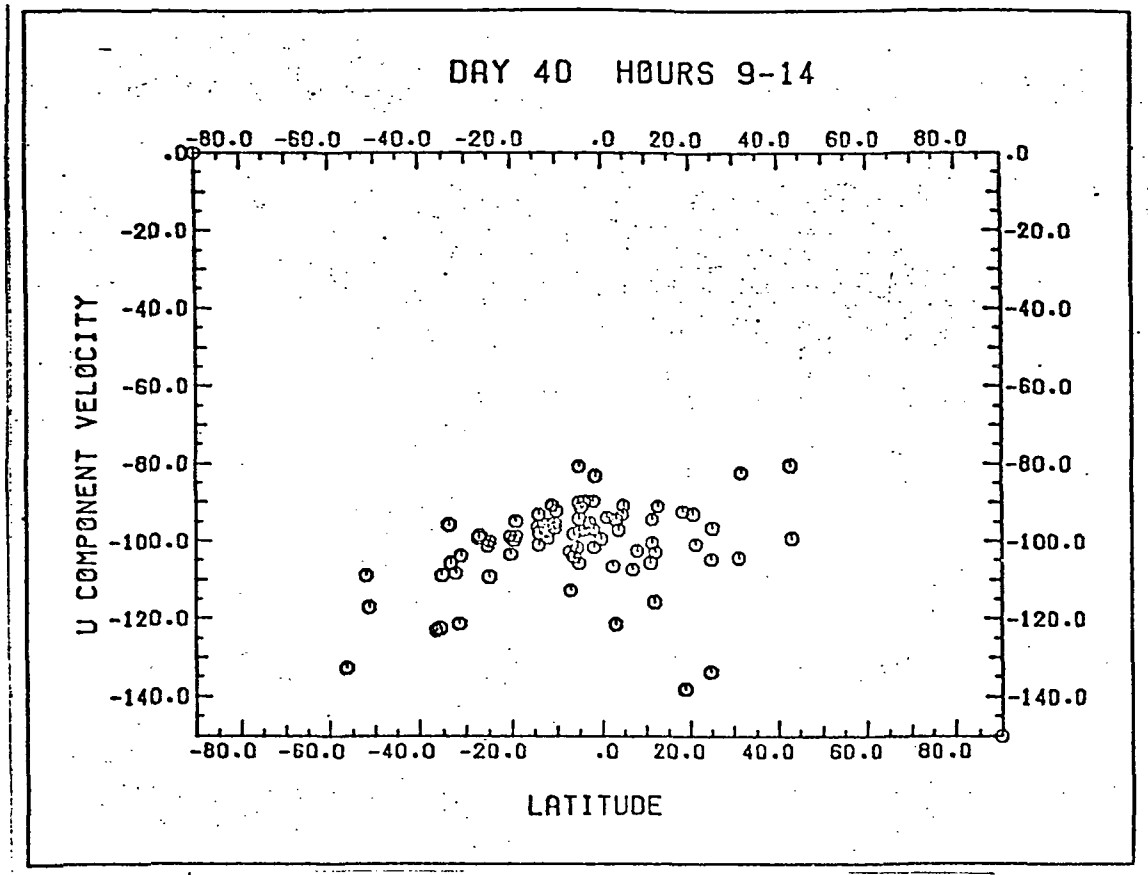

Figure 1e. Unedited measurements for set III.

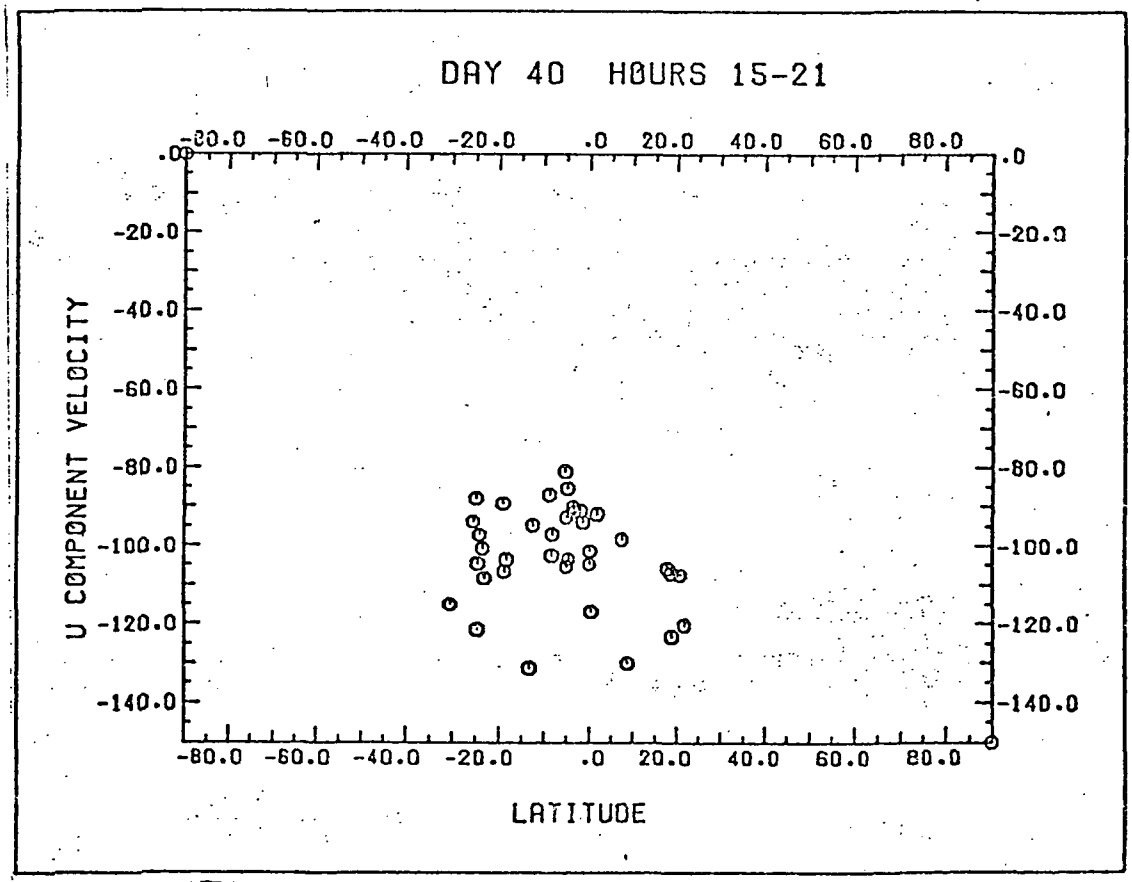

Figure 1f. Unedited measurements for set IV.

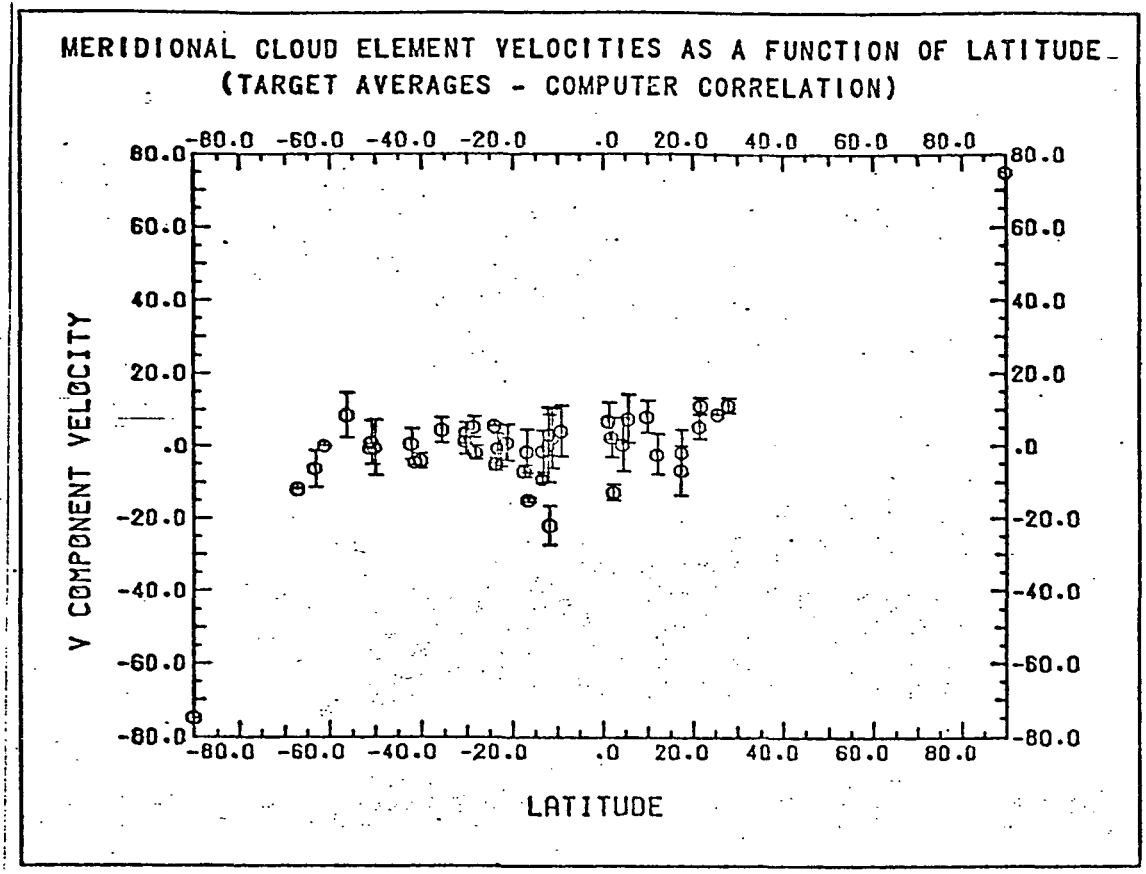

Figure 2a. Target averages for 15 m/s edited measurements -- data set I.

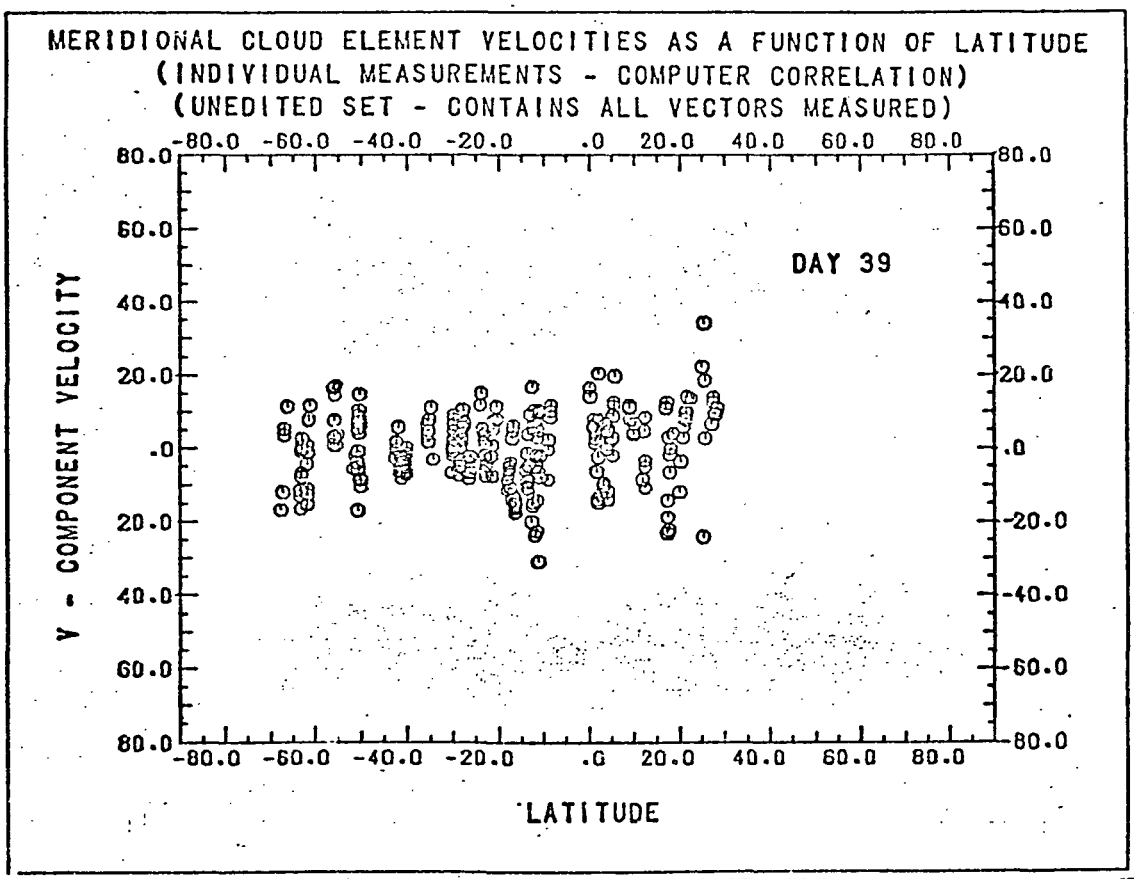

Figure 2b. Unedited measurements for day 39 (data set I). Compare with Figure 2c and with Figures 2 d-f.

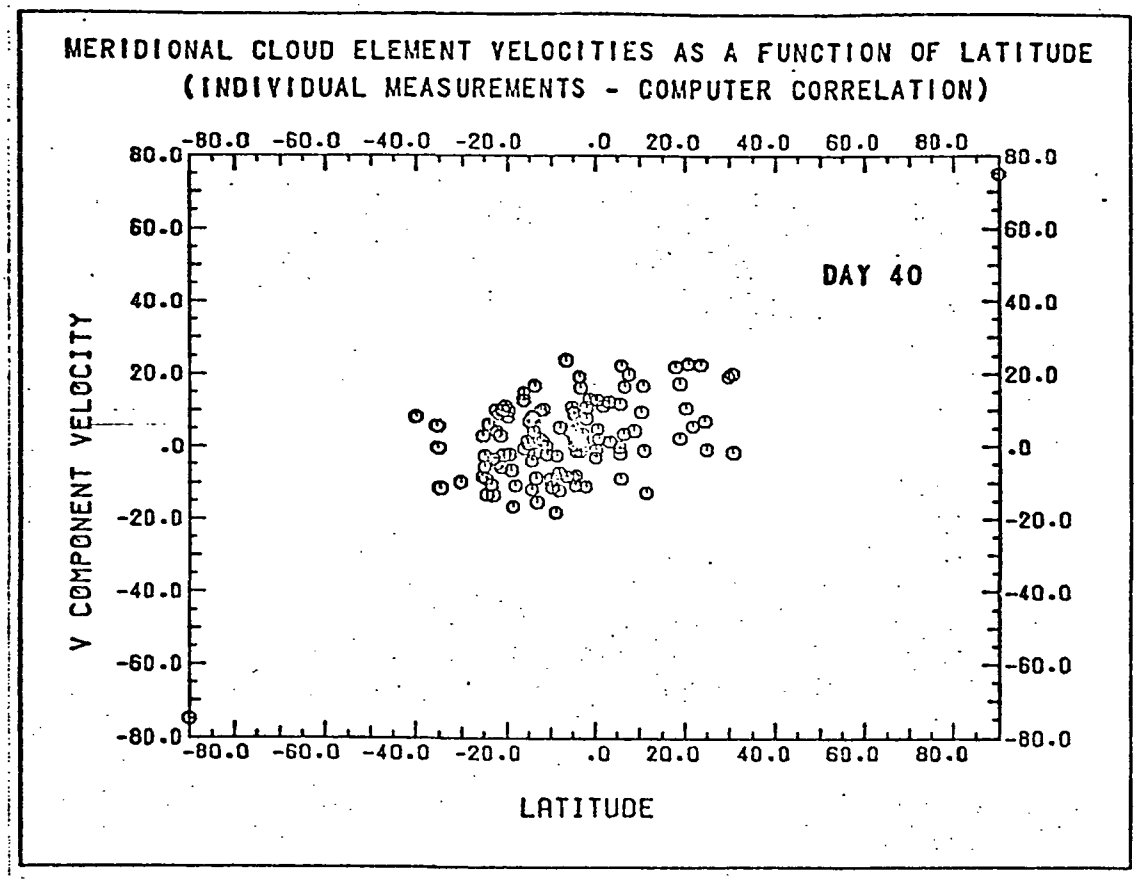

Figure 2c. Unedited measurements for day 40 (data sets II, III, IV, combined).

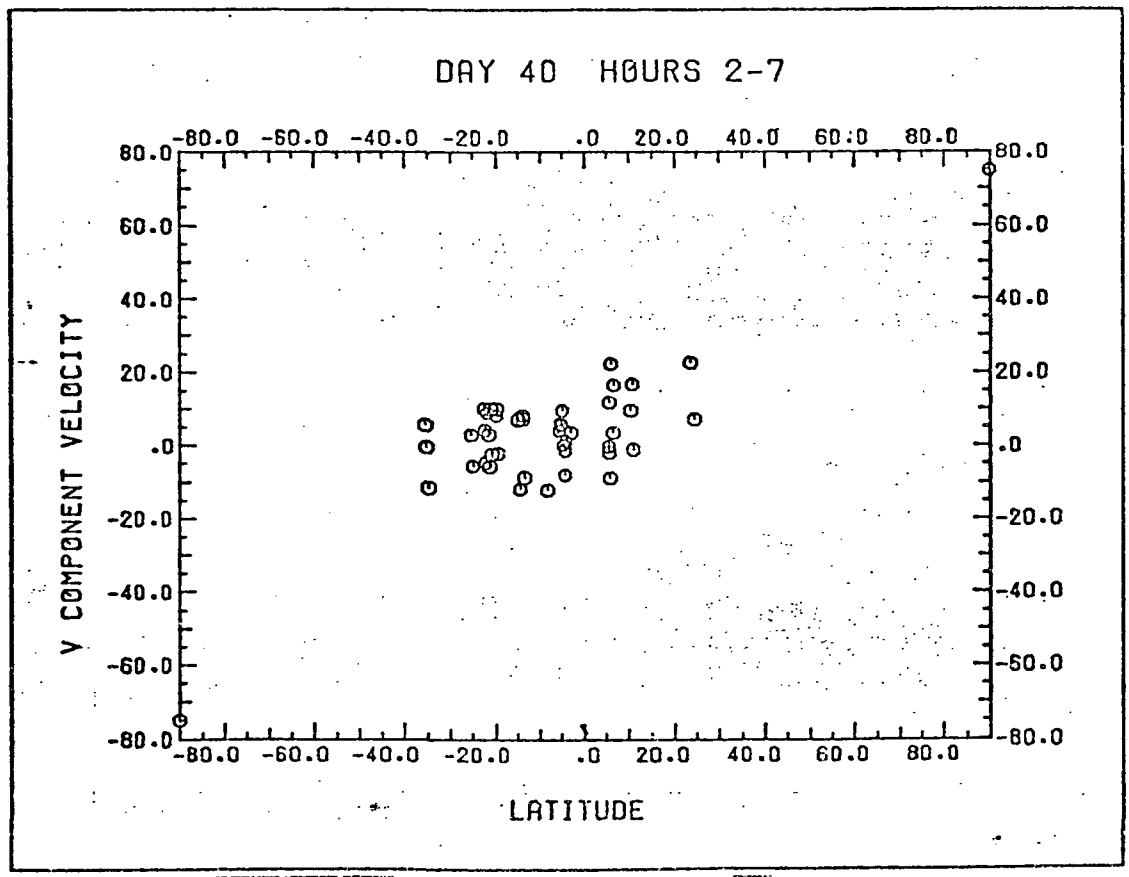

Figure 2d. Unedited measurements for data set II.

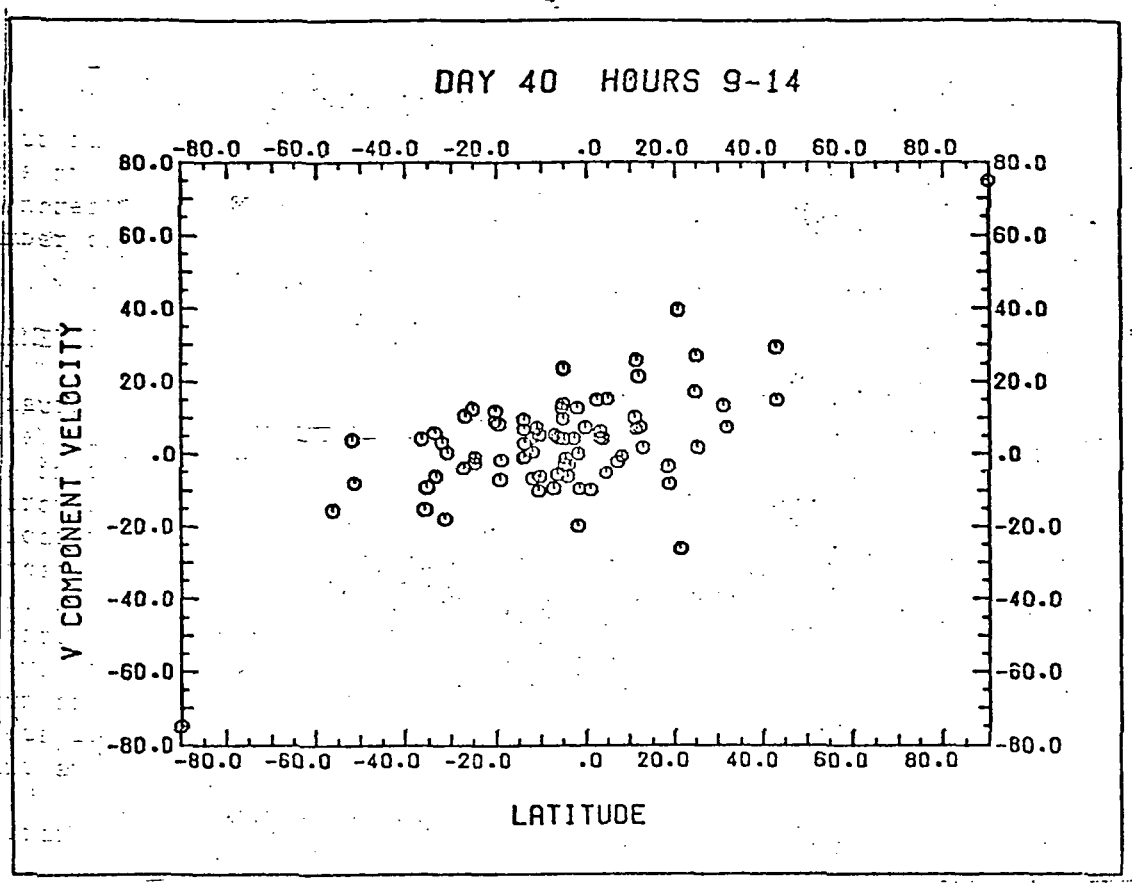

Figure 2e. Unedited measurements for data set III. Note how the slope of the distribution changes from Figure 2d to Figure 2f.

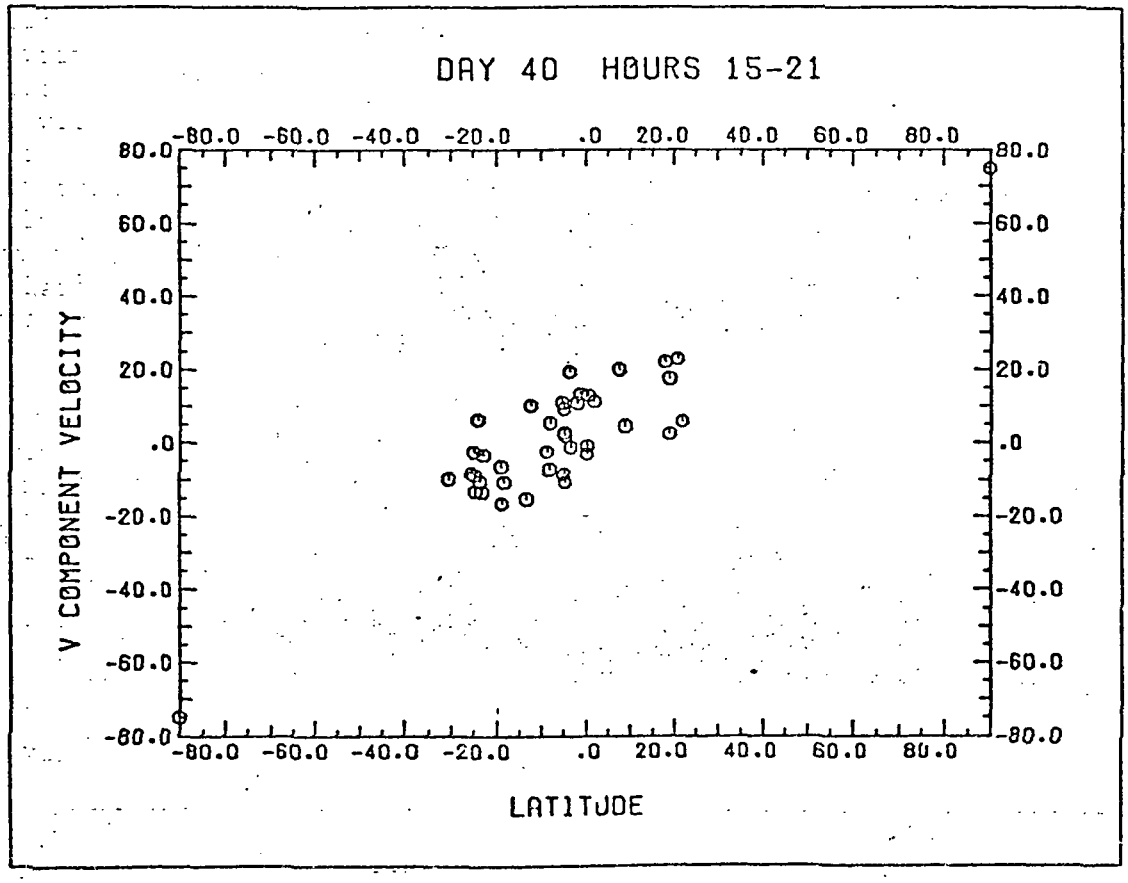

Figure 2f. Unedited measurements for data set IV.

harder to find and track, there is a higher proportion of correlation failures by the computer and the scatter in the remaining good measurements increases. With greater care and effort, we may eventually double the number of acceptable vectors obtained from day 40.

MEASUREMENTS OF CLOUD MOTION

Figure 1 contains plots of u-component (zonal) velocities versus latitude. In data set I (Figure 1a) there were enough high resolution details in the clouds to get velocities above 45° latitude and show the sharp dropoff at constant angular velocity as one approaches the pole. The velocity maximum at 45° is clearly defined, as is the small subset of six targets appearing to move at constant angular velocity (along the dotted line) at low and mid latitudes. The majority of targets in the low and mid latitudes show a velocity profile which gradually increases as one moves away from the equator. This indicates a tendency to conserve angular momentum about the poles and this differential motion is also present in data sets II, III, and IV, as well. Note that there is no group of slow, constant angular velocity points as in set I. Scatter in the measurements is somewhat greater on day 40 in the proportion one would expect from the poorer resolution in the image.

The meridional velocity gradient is seen in Figure 2, appearing as a slope to the distribution in the plots. Note that there is a definite increase in slope from day 39 to day 40 (Figures 2b and 2c) and that throughout day 40, the slope continues to increase (Figures 2d, 2e, 2f). Data set IV (Figure 2f) does not have enough good measurements at high latitudes. This lack of successful image correlations at high latitudes is due primarily to poorer resolution, which makes finding and tracking small cloud targets more difficult and more subject to correlation failures. Coupled with the increased measurement scatter, the result of the poor resolution in Figure 2f is a slope of the points in the plot which is probably twice as large as it should be. This degradation of data can be partially offset by a greater effort to get better measurements from the data, but we believe that as resolution gets worse, it will be necessary to choose larger and larger albedo features to track, since small cloud features such as edges and minor convective elements will no longer be visible.

The longitudinal velocity gradient of the zonal winds shows a definite drop from day 39 to day 40. Indeed, the gradient on day 40 appears to be nonexistent (Figure 3c). Lower or equal velocities at the evening terminator cannot be explained in terms of a target selection bias due to viewing geometry (as the higher velocities on day 39 could be explained), so we conclude that the reduction in slope is real. That this is an actual physical trend we are observing, and not a statistical deviation, is evident from Figures 2d, 2e, and 2f, which show that the longitudinal gradient does not merely disappear on day 40, but is undergoing a change in sign. As discussed in Krauss (1976), other experimenters have also seen higher velocities at the evening terminator. This is the first observation of lower zonal velocities at the evening terminator, and has profound

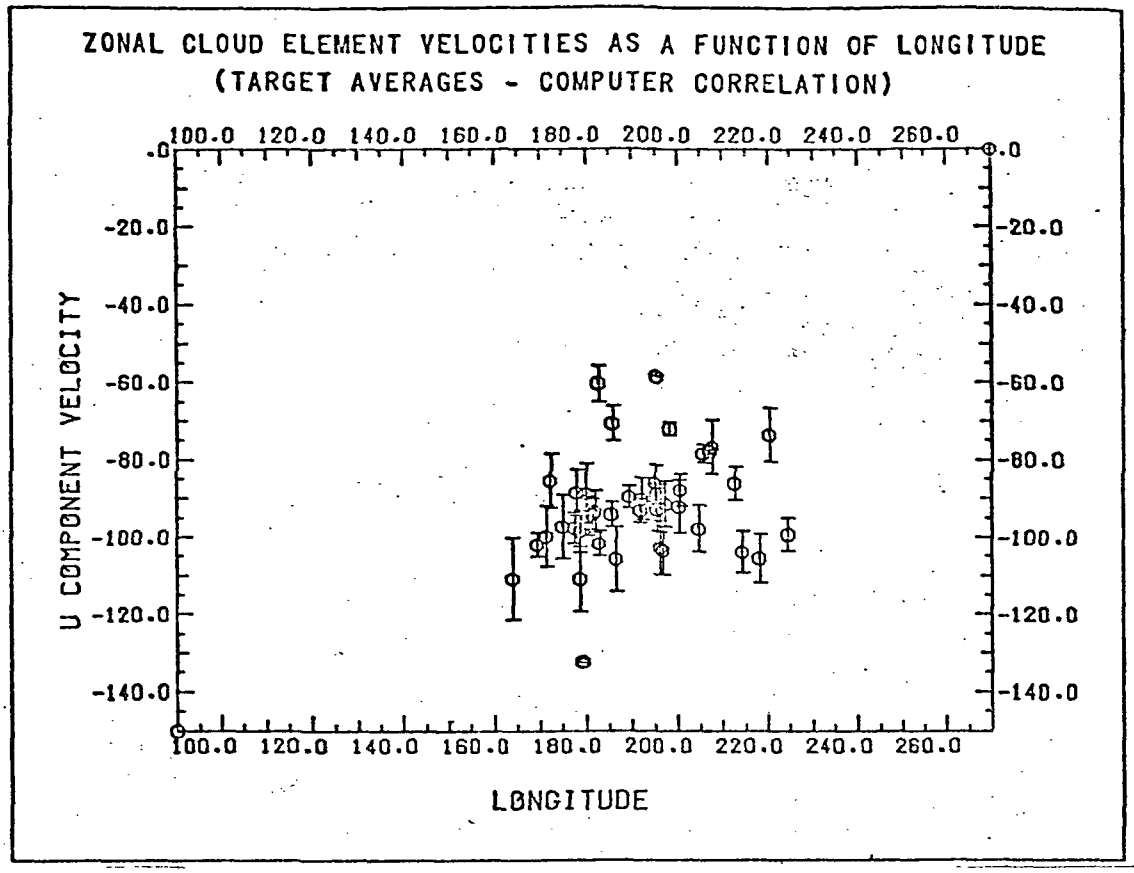

Figure 3a. Target averages for 15 m/s edited measurements -- data set I.

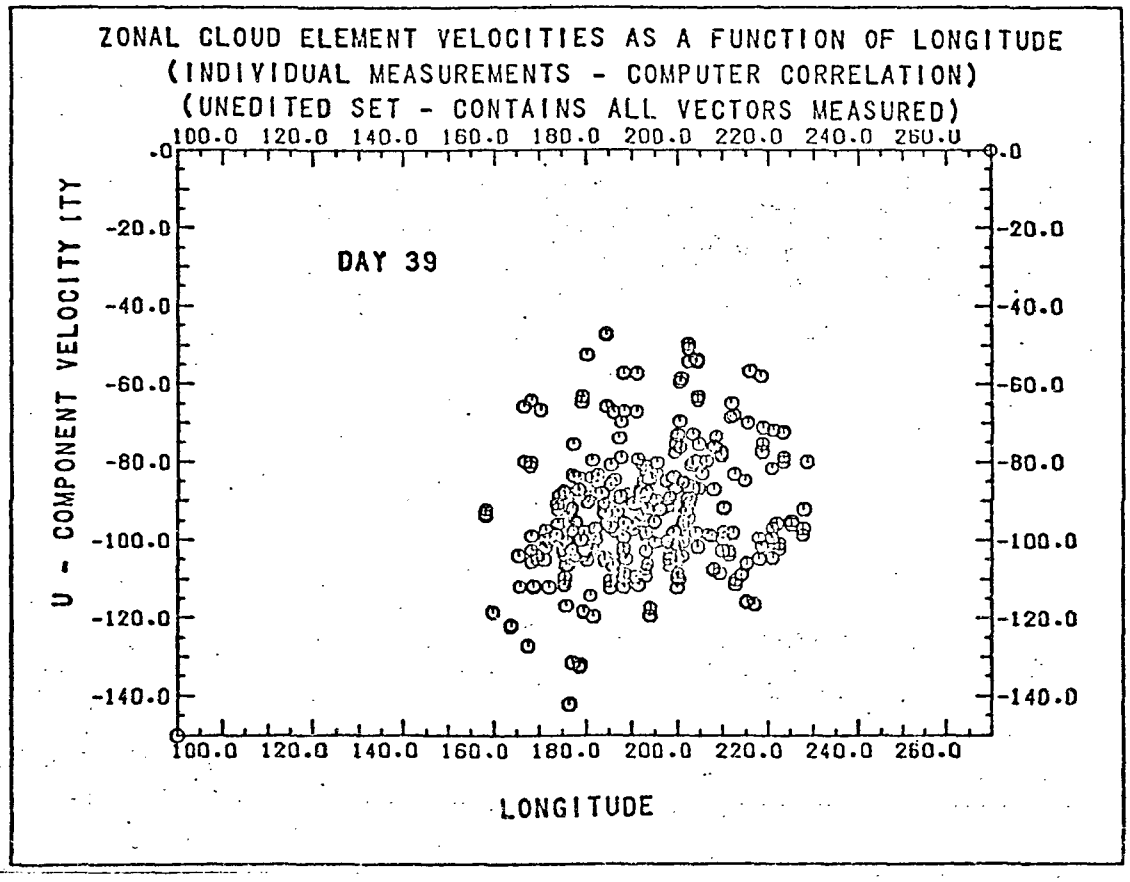

Figure 3b. Unedited measurements for day 39 (data set I). Compare with Figure 3c and Figures 3 d-f.

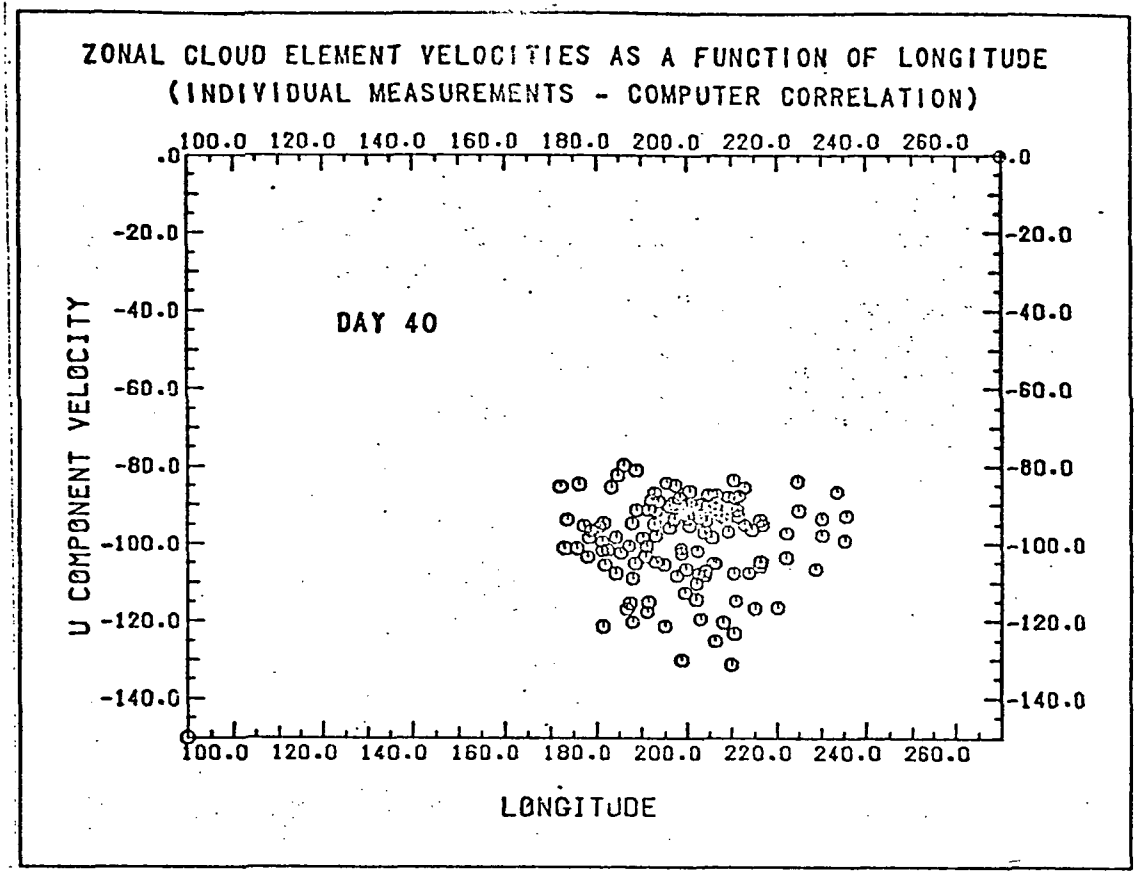

Figure 3c. Unedited measurements for day 40 (data sets II, III, IV, combined).

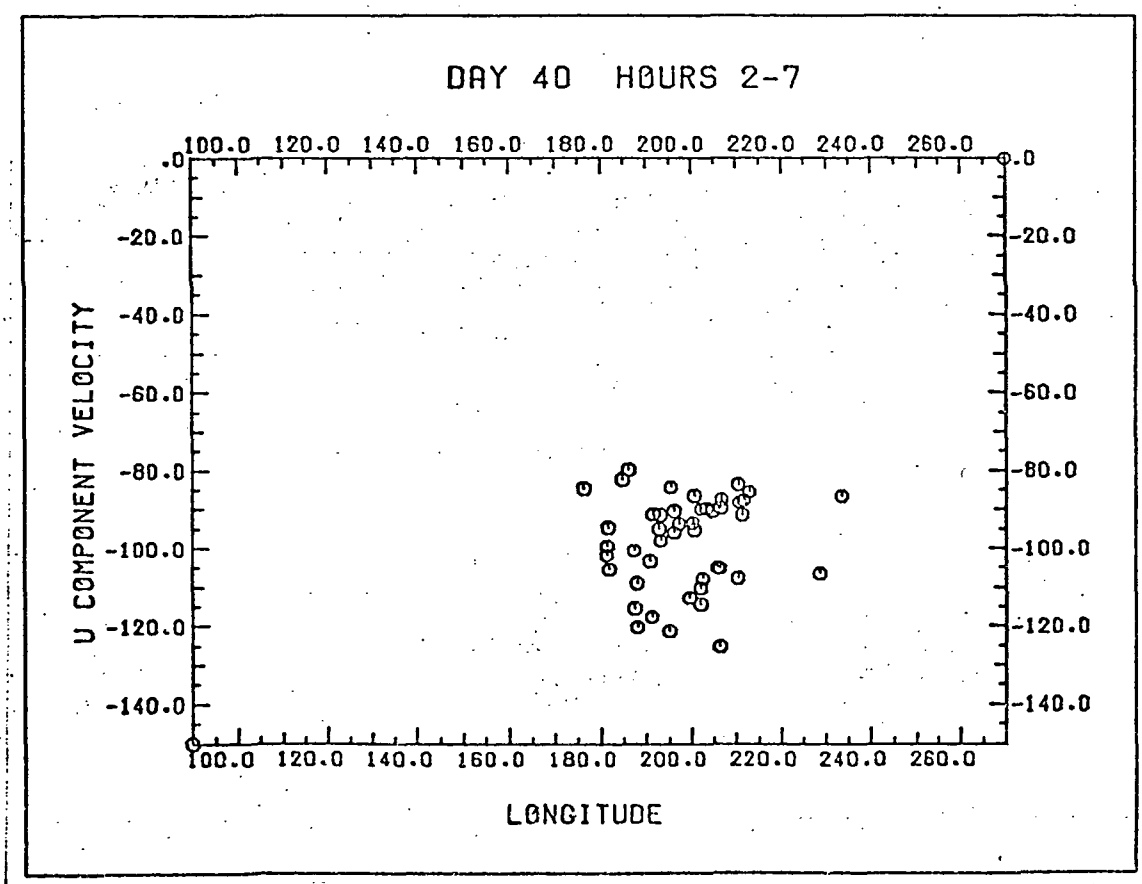

Figure 3d. Unedited measurements for data set II.

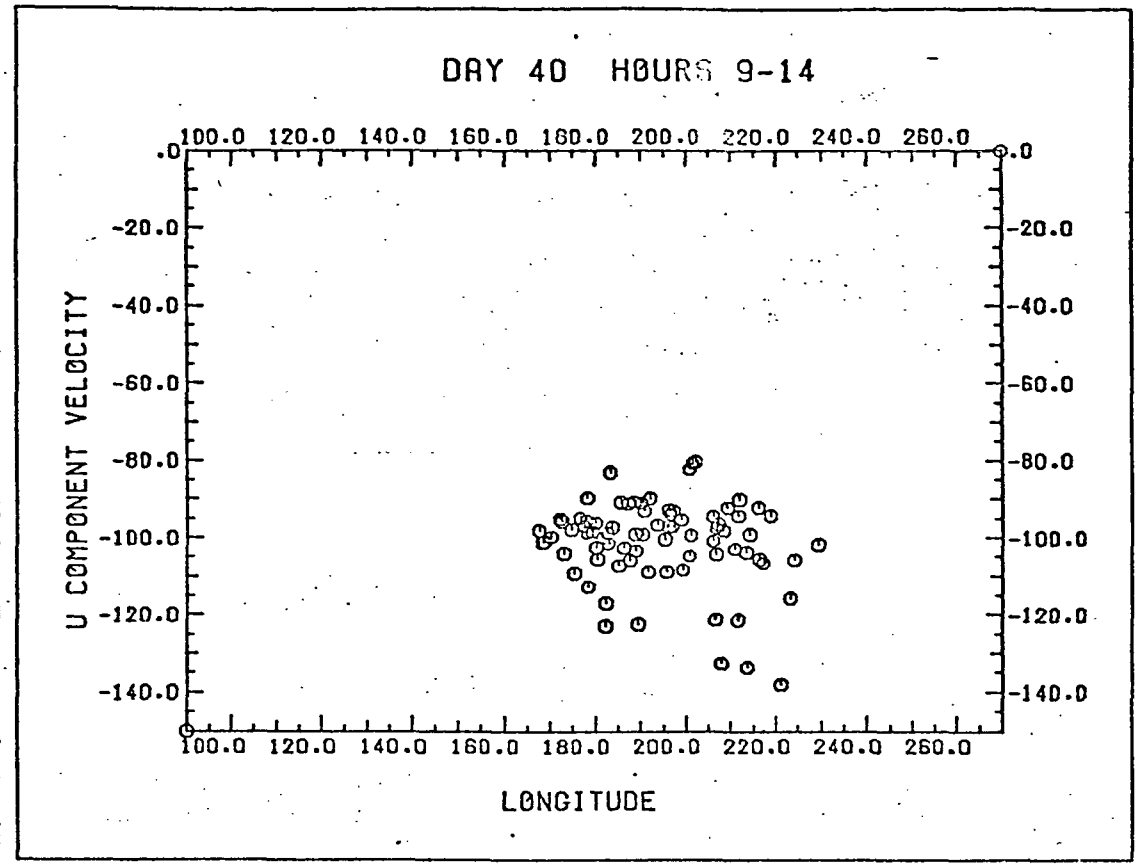

Figure 3e. Unedited measurements for data set III. Note how the slope of the distribution changes from Figure 3d to Figure 3f.

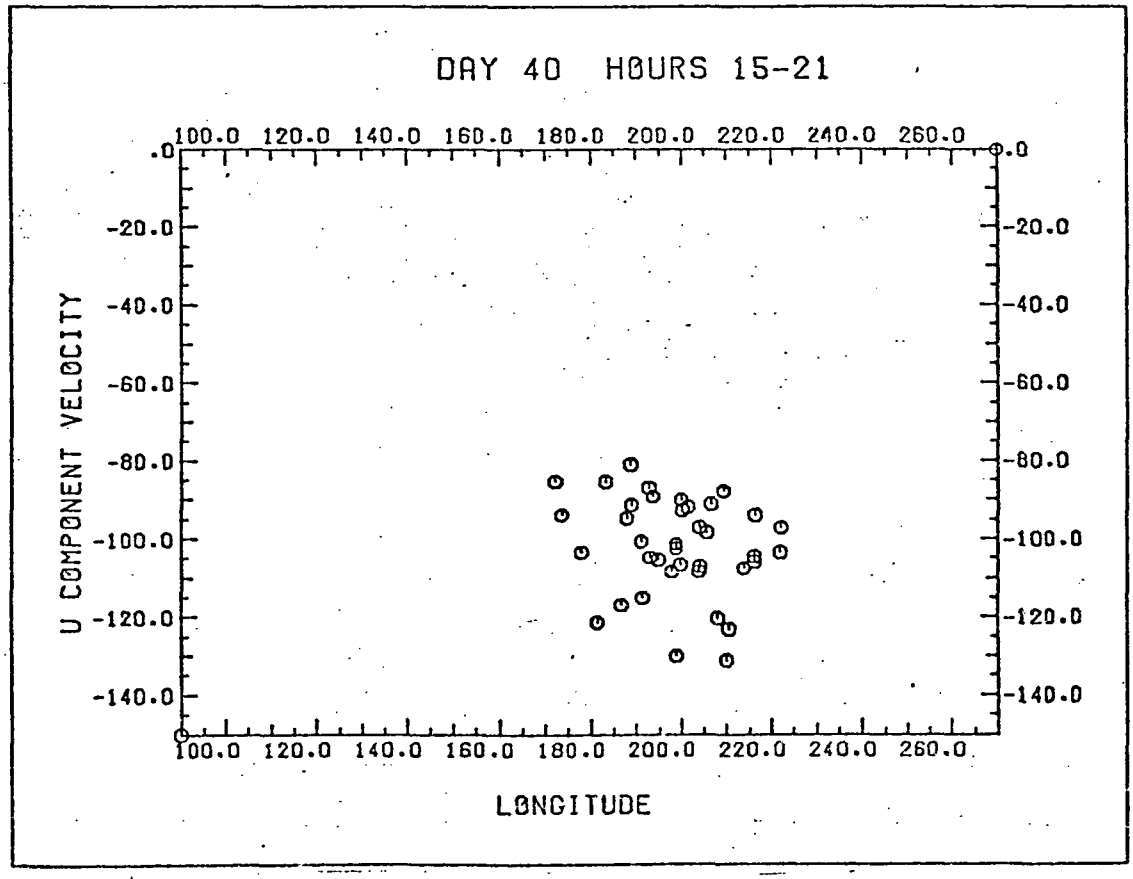

Figure 3f. Unedited measurements for data set IV.

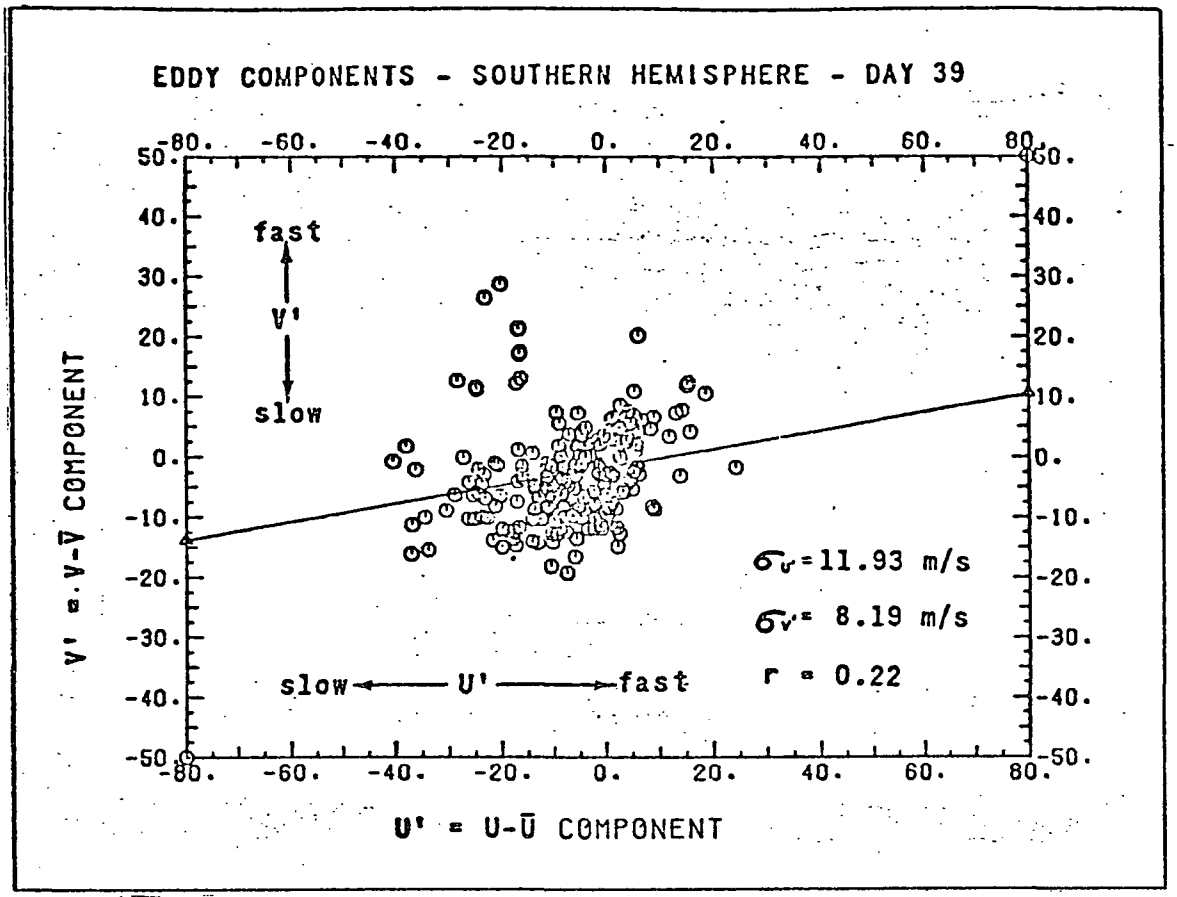

Figure 4a. Eddy transport in southern hemisphere (day 39).

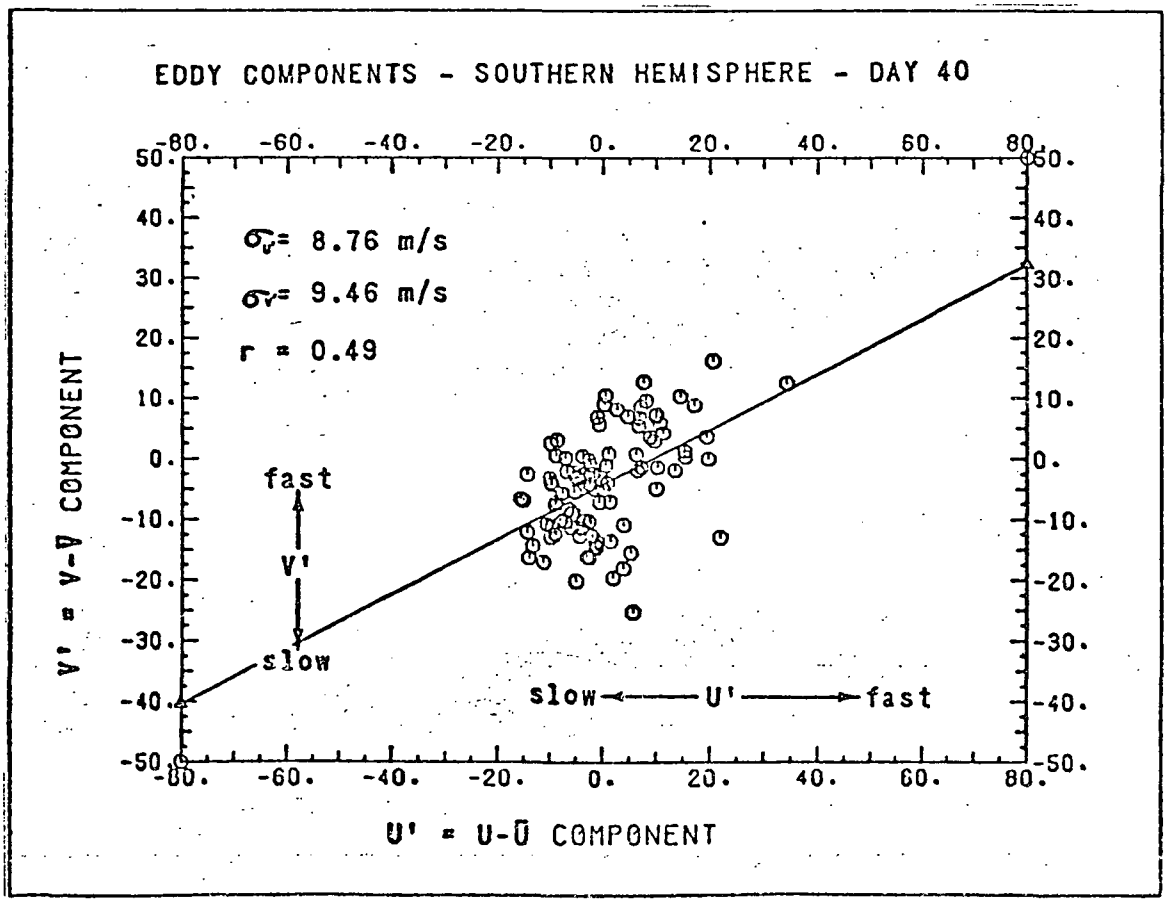

Figure 4b. Eddy transport in southern hemisphere (day 40).

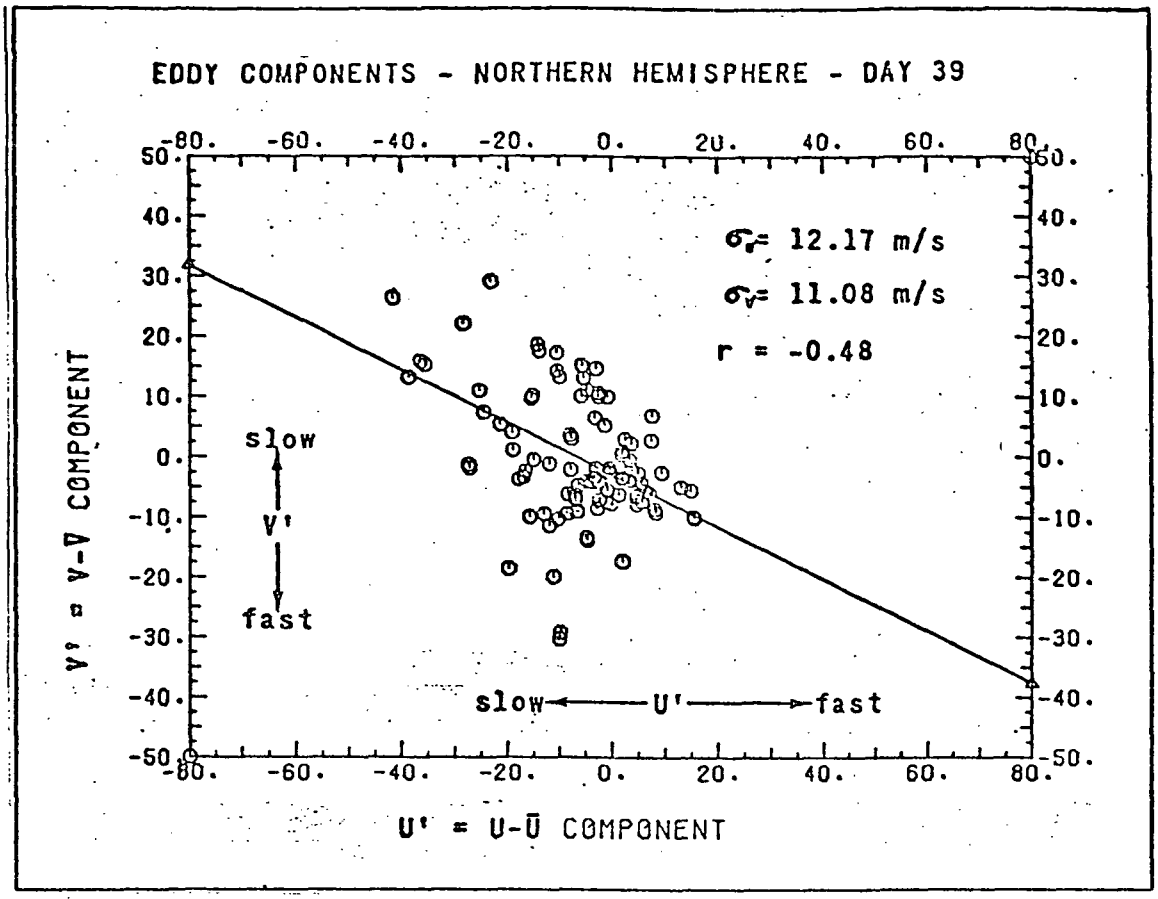

Figure 5a. Eddy transport in northern hemisphere (day 39).

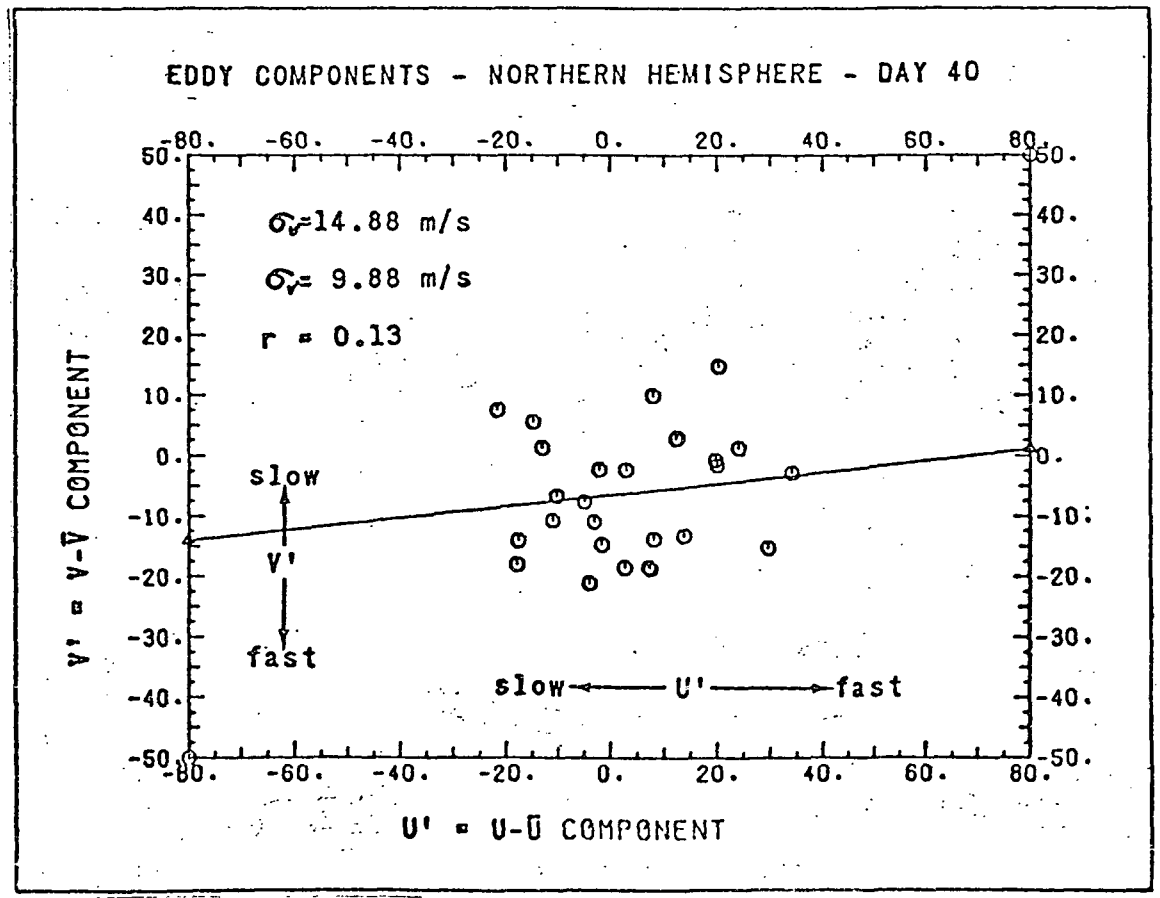

Figure 5b. Eddy transport in northern hemisphere (day 40). This is the only correlation plot indicating equatorward momentum transport. Correlation is low, however, and measurements too few for confidence.

implications for explanations of the drive for the zonal winds. Solar tides and Reynolds stress theories require a sun-locked zonal velocity field. If velocities at the terminator are occasionally lower, the drive for the zonal winds cannot be sun-locked.

No change of the meridional velocities with longitude was observed in any data set. Least squares fits showed no slope to within 2 m/s over the entire longitude range measured.

EDDY MOTIONS

It is possible, using the measured u and v profiles, to investigate the transport of zonal momentum along a meridian. One computes a mean $\bar{u}$ and $\bar{v}$ as a function of latitude and subtracts it from the u and v components of each measured velocity vector. What is left must be the residual components u' and v', respectively. If there is no organization to the residual flow, u' and v' will be randomly scattered around the origin. One could then assume that the scatter is due to measurement uncertainty, random cloud motions, convection, etc. The displacement of the center of mass of the distribution and the increase in $\sigma_{u'}$ over σ_u and $\sigma_{v'}$ over σ_v are measures of how accurately $\bar{u}$ and $\bar{v}$ were chosen as a function of latitude, so the $\bar{u}$ and $\bar{v}$ choice need not be perfect, merely reasonable enough to keep the scatter from growing significantly.

If one finds a non-zero correlation in the scatter plots, however, that means that the faster u' are associated with the faster v' (poleward zonal momentum transport) or the slower u' are associated with the faster v' (equatorial zonal momentum transport). Figures 4 and 5 show the results of such an analysis. In the southern hemisphere (Figure 4), the correlation coefficient, r, is 0.22 on day 39 and 0.49 on day 40. In the northern hemisphere (Figure 5), v and r must change sign, but we still find a correlation of -0.48 on day 39. Day 40 shows a very slight equatorward momentum transport, but it should be remarked that there are only a few points in the plot, widely scattered, and we really ought to have better statistics. One would not change $\sigma_{u'}$ and $\sigma_{v'}$ very much by tilting the least squares fit to a negative correlation in Figure 5b. On the whole then, momentum transport seems to be toward the poles in the plots.

The total momentum transport is given by the sum of the mean flow transport and the eddy transport:

$$\overline{uv} = \bar{u}\,\bar{v} + u'v'r$$

$$= 93 \text{ m/s} \cdot 6 \text{ m/s} + 5 \text{ m/s} \cdot 3 \text{ m/s} \cdot 0.4$$

where we have substituted representative mean values for the quantities in the equation. Even if u' and v' are estimated wrong by several hundred percent, it is clear that the eddy transport toward the poles is still considerably smaller than transport by the mean flow.

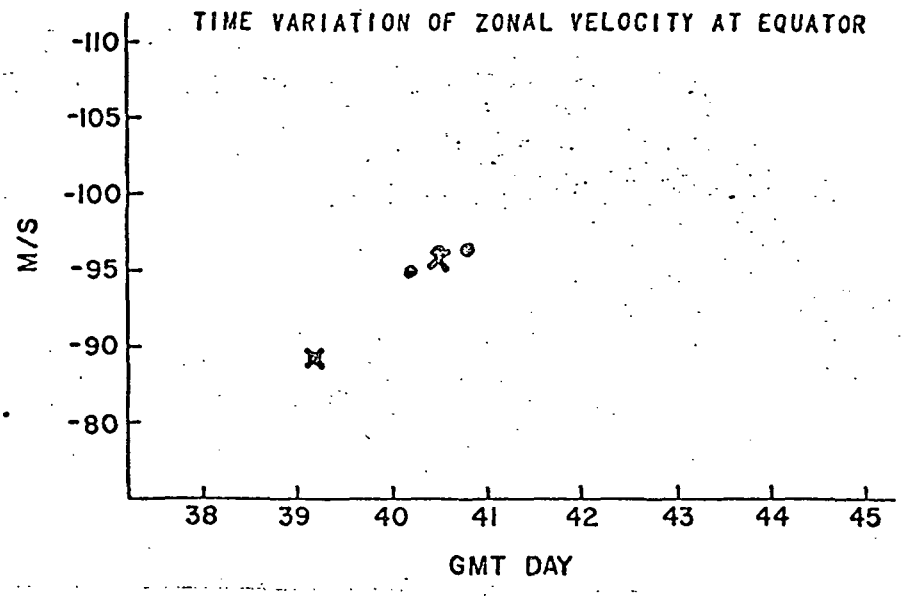

Figure 6. Zonal velocity of the upper atmosphere of Venus at the equator increases by about 5 m/s from day 39 to day 41. The velocity is determined by the minimum in a second order polynomial least squares fit to all cloud motion measurements between +45° and -45° latitude.

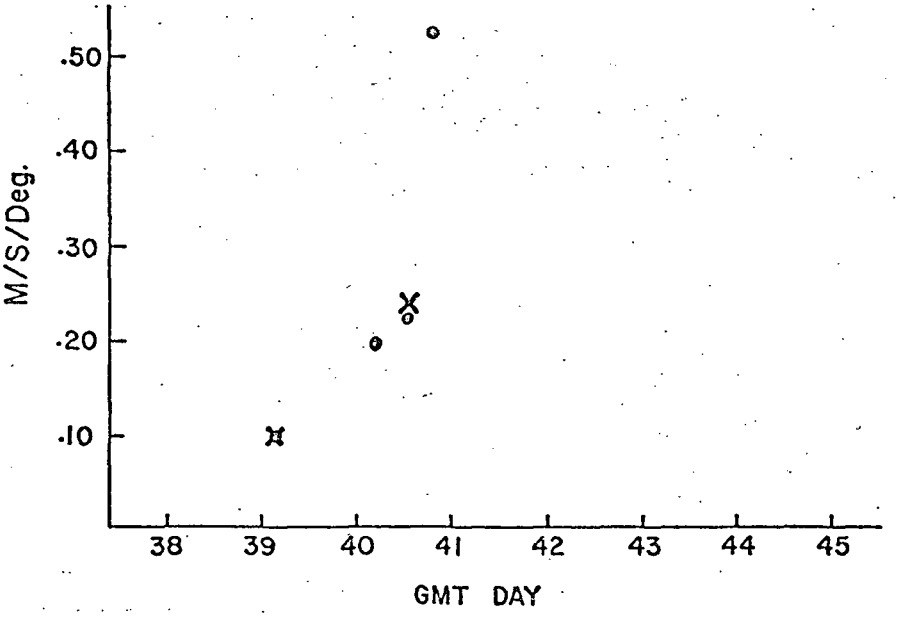

Figure 7. The meridional velocity, which is directed away from the equator in each hemisphere, tends to accelerate as it approaches higher latitudes. The rate of increase is substantially higher on day 40 than on day 39.

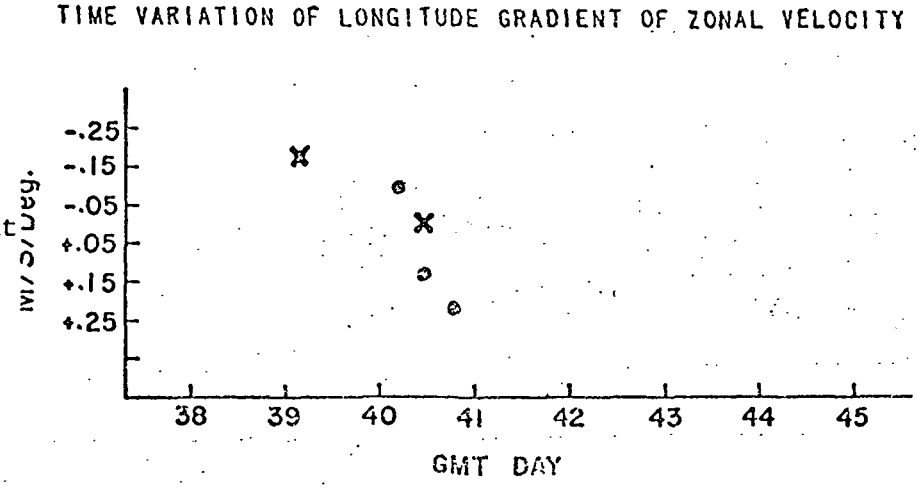

Figure 8. The zonal velocity may increase in time from day 39 to day 41, but it shows a negative gradient with respect to longitude on day 39 (faster speed at the evening terminator), and changes to a positive gradient through day 40 (slower speeds at the evening terminator). Note that there is a high degree of correlation of changes shown in Figures 6, 7, and 8.

Suppose the dynamic coupling is due to a large scale wave. The eddy component transport indicates that there is some kind of global scale organization in the deviations from the mean flow. This same organizational structure could be visible in the correlation of trends in the horizontal velocity measurements and velocity gradients, although there is no evidence that they are related. We can, however, speculate how a global scale wave might transport momentum upward by assuming that the measured divergence at the start of day 39 is coupled to rising motion near the equator. In the simplest case, this involves using only the equation of continuity. Then vertical motion, $+w'$, is correlated with increasing zonal velocity, $+u'$.

Now we make another "reasonable" assumption not yet supported by any evidence. Suppose, considering how the correlated velocities fluctuate, that we have relative convergence at some later time. We are assuming that u' and v' will thus both decrease together in time. Then, by continuity, we should have sinking motion near the equator. In actuality, because the vortex flow is dominant, we merely have reduced rising motion. The result is the same, however, for then $-w'$ is coupled to $-u'$. The product in both cases ($+w' \cdot +u'$ and $-w' \cdot -u'$) is positive, so, following the same argument as before for the eddy transport due to $u'v'$, we can say that zonal momentum is transported upward near the equator.

Now, identifying what kind of wave or combination of waves couples u, v, and w in the proper phase relationship and with the proper period will take further study. The simplest picture would have the upper atmosphere vortex spinning like a global scale taffy pull with a single pressure bulge centered on the equator and moving around the planet with a period close to that of the 4 day UV cloud motions.

Clearly, the next most important step is to extend the velocity field measurements to earlier and later times to determine the period and amplitude of the velocity fluctuations and to see if the correlation in the measurements is maintained. We cannot go beyond day 40 because the time resolution of the Mariner 10 data was cut to 8-12 hours and is not suitable for small scale motion measurements. Consequently, it would appear that we must concentrate on day 38, and possibly 37 (as close as our existing navigation scheme will permit before it breaks down). Another area of study will be an intensive look at the characteristics of other wavelike features on Venus -- the bowlike waves, circumequatorial belts, etc. -- and at vertical structure of the UV clouds. We must determine what influences the velocity fields, where, when, and how much. This task will also require detailed analysis of the higher resolution Mariner 10 imagery.

ACKNOWLEDGEMENTS

The author wishes to thank V. E. Suomi for suggesting the search for eddy transport and Sanjay Limaye for navigating the images. The manuscript was typed by Rosanne Koehler.

This research was supported by NASA Grant #NGR-50-002-189 and JPL Contract #953034.

BIBLIOGRAPHY

Krauss, Robert J.; 1976: "UV Cloud Motions on Venus From Mariner 10 Images," SSEC Report on Atmospheric Dynamics of the Planets, Vol. 1.

Suomi, Verner; 1975: "Cloud Motions on Venus," in The Atmosphere of Venus, NASA SP-382, p. 42-58.

Appendix B

PREPRINT

VENUS ATMOSPHERE: DRY ADIABATIC DIAGRAMS AND OBSERVED THERMAL STRUCTURE

Sanjay S. Limaye and Verner E. Suomi

Department of Meteorology
University of Wisconsin, Madison

Submitted to the

Journal of Atmospheric Science

June 1976

VENUS ATMOSPHERE: DRY ADIABATIC DIAGRAMS AND OBSERVED THERMAL STRUCTURE

Sanjay S. Limaye and Verner E. Suomi
Dept. of Meteorology, University of Wisconsin, Madison

ABSTRACT

The dry adiabatic lapse rate γ_{ad} for an atmosphere of different mixtures of carbon dioxide and nitrogen (20%, 16%, 12%, 8%, 4%, and 0% nitrogen by mass) is computed as a function of temperature and pressure and an adiabatic diagram depicting the dry adiabatic temperature changes constructed. Following Staley (1970) the real gas expression for the dry adiabatic lapse rate is used incorporating the tabulated values of the specific heats of nitrogen and carbon dioxide. A four point Lagrangian interpolation scheme as recommended by Hilsenrath et al. (1960) is used to minimize interpolation errors in the specific heats and compressibility factors at intermediate pressures and the variation in the acceleration due to gravity with altitude is included in the computation.

The results indicate that the dry adiabatic lapse rate is about $7.98 K \cdot km^{-1}$ at 93 atm pressure (= surface pressure on Venus) and 740K and increases to about $10.25 K \cdot km^{-1}$ at 1.0 atm pressure and $T \doteq 300K$ for a 4% nitrogen and 96% carbon dioxide atmosphere. At a given pressure the dry adiabatic lapse rate magnitude is seen to increase with pressure and decrease with increasing amounts of nitrogen for the same pressure and temperature.

Comparisons of the temperature profiles obtained from Veneras 4 through 8 and Mariners 5 and 10 against the dry adiabatic diagrams indicate a transition layer at about 3-5 atmospheres level ($\sim$38 km altitude) wherein

the lapse rate changes from a neutral value to a very stable one above that level. This agrees with the lower limit level for maximum solar energy deposition suggested (Lacis, 1974).

Below this transition layer the atmospheric stability appears to be neutral although inconclusively so due to (i) experimental errors in T(P), (ii) uncertainty in the adiabatic temperature changes, due to errors in $C_p(P,T)$ and Z(P,T), and (iii) uncertain atmospheric composition. Up to 20% of nitrogen by mass must be added to the CO_2 atmosphere to make the observed profile neutrally stable if the first two terms are small. Other gases of lower specific heats will also have a similar effect.

The stability of the lower atmosphere to vertical displacements is still uncertain. If indeed the lower atmosphere is neutral, then perhaps the assumed atmospheric composition is in error. Latent heat release only lowers the adiabatic (moist) lapse rate and makes the atmosphere more unstable.

1. Introduction

Whether the observed lapse rate of temperature in planetary atmospheres is equal to the adiabatic value is an important factor in the atmospheric motions. In the case of the terrestrial atmosphere one assumes ideal gas behavior, thus the dry adiabatic lapse rate is easily defined as the ratio g/C_p where g is the acceleration due to gravity and C_p is the specific heat of air at constant pressure. It was indicated by Staley (1970) that this definition is not readily applicable for the atmosphere on Venus because at much higher pressures the atmospheric state is far from ideal. An expression derived for a real gas is needed to specify the dry adiabatic lapse rate of temperature on Venus, once the atmospheric composition is known. Unfortunately, we do not know the exact composition of the Venusian atmosphere.

The vertical thermal structure of the Venusian atmosphere has been probed so far by seven Russian capsules in the Venera series which have descended in the atmosphere and remotely through the radio occultation technique by the American spacecrafts Mariner 5 and Mariner 10. (Avduevsky et al., 1970, 1971; Marov et al., 1973: Howard et al., 1974) The atmospheric composition, however, has only been estimated at pressures less than about 10 atmospheres from the Russian entry probes Veneras 4, 5, and 6. The composition indicated is up to about 97% carbon dioxide and the rest predominantly nitrogen, up to about 8% (Vinogradov et al., 1968; Marov, 1973).

Based on this approximate atmospheric composition, all the temperature profiles have been generally interpreted to be mostly adiabatic. However, the "standard", i.e. the value of the adiabatic lapse rate itself varies with temperature, pressure and atmospheric composition and thus the vertical thermal structure needs to be studied further.

It is interesting to note that on careful scrutiny of the temperature profiles, superadiabatic regions are suspected (Fjeldbo et al., 1971; Avduevsky et al., 1968; Ainsworth et al., 1974). Indeed, the experimental conditions during descent may cause the measurement errors to be greater than those measured in the laboratory, yet the doubts of a superadiabatic region in the lower atmosphere cannot be completely eliminated as a reinterpretation of the Venera 8 profile also indicates (Ainsworth and Herman, 1974).

This paper describes an attempt to specify the magnitude of the dry adiabatic lapse rate for a given atmosphere which is a mixture of nitrogen and carbon dioxide at conditions found in the atmosphere of Venus.

In the following sections the considerations which went into the construction of the adiabatic diagram based on a real gas definition of specific heat are described. It should be pointed out here that except for the case of 100% carbon dioxide, the dry adiabatic lapse rate calculation for a mixture of carbon dioxide and nitrogen is based on a simplistic approach that the molecular interactions at the high temperatures and pressures of one gas component on the other in the lower atmosphere of Venus are negligible in terms of their influence on the dry adiabatic temperature changes. Molecular interactions of the same species are converted. We then compare the measured (T,P) profiles for the atmosphere of Venus against these values of the dry adiabatic lapse rate to infer about the static stability.

2. Construction of the Adiabatic Diagram

Staley (1970) has pointed out that the ideal gas definition $\gamma_{ad} = g/C_p$ is not applicable in the case of Venus because of large deviations of the atmosphere from idealness. As a result, the specific heat at constant pressure cannot be taken to be constant. Fig. 1 shows the variation of

the specific heat of carbon dioxide at constant pressure under the conditions found in the atmosphere of Venus.

For a real gas, the dry adiabatic lapse rate can be shown to be (Staley, 1970):

$$\gamma_{ad} = -\frac{dT}{dz} = -\frac{T(\partial p/\partial T)_\alpha}{(\partial p/\partial \alpha)_T}\left(\frac{g}{C_p}\right) = \frac{T(\partial p/\partial T)_\rho}{\rho(\partial p/\partial \rho)_T}\left(\frac{g}{C_p}\right) \qquad (1)$$

where α: specific volume

ρ: density $= \frac{1}{\alpha}$

g: acceleration due to gravity

The hydrostatic assumption is made in arriving at the above expression. Values of thermodynamic variables for carbon dioxide and nitrogen are found in a compilation by Hilsenrath et al. (1960). The deviation of the tabulated values from direct measurements is generally less than 2% for specific heats of carbon dioxide and nitrogen and about 0.5% for their tabulated values for density and compressibility.

The expression for γ_{ad} can be transformed into a form involving the compressibility factor Z, through the use of the virial equation of state:

$$\frac{\alpha p}{RT} = 1 + \frac{B(T)}{\alpha} + \frac{C(T)}{\alpha^2} + \ldots\ldots = Z \qquad (2)$$

where B(T) and C(T) ... are the virial coefficients. Following Staley (1970):

$$T(\partial p/\partial T)_\rho = \frac{p\left[\frac{\partial}{\partial T}(TZ)_p\right]}{Z - p(\partial Z/\partial p)_T} \qquad (3)$$

and

$$\rho\left(\frac{\partial p}{\partial \rho}\right)_T = \frac{pZ}{Z - p(\partial Z/\partial p)_T} \qquad (4)$$

so that

$$\gamma_{ad} = \frac{1}{Z}\left[\frac{\partial}{\partial T}(ZT)\right]\frac{g}{C_p} \qquad (5)$$

or equivalently,

$$\gamma_{ad} = -\frac{T}{\rho}\left(\frac{\partial \rho}{\partial T}\right)_p \frac{g}{C_p} \qquad (6)$$

However, this form offers no advantage over the one involving the compressibility factor for computational purposes since the tabulated values of density and the compressibility factor have been made internally consistent (Hilsenrath et al., 1960).

The thermodynamic values needed for calculation are tabulated at 0.01 and n(0.1, 0.4, and 0.7) atmospheres pressure (where n = 1, 10, 100) up to 100 atmospheres and at every 10K interval from generally 200K to 1500K. (See Figs. 2 and 3 for Z(p,T) for carbon dioxide and nitrogen respectively.)

The adiabatic diagram was then constructed using expression (5) follows: the value of $\gamma_{ad}(T_o,p_o)$ was first computed at an initial point T_o and p_o. T_o was varied from 1000K to 700K and p_o was fixed at 100 atmospheres. The temperature T at a pressure p-Δp is computed using the previous value of the lapse rate. The compressibility factor at this new pressure level and temperature was then computed from the tabulated values by a linear interpolation for temperature and four point Lagrangian interpolation (Conte, 1965) for pressure, in order to minimize the errors introduced by linear interpolation for pressure as suggested by Hilsenrath et al. as follows:

$$f(p) = \sum_{k=0}^{n} L_k(p) f_k \qquad (7)$$

where L_k are the polynomials:

$$L_k(p) = \prod_{\substack{j=0 \\ j\neq k}}^{n} (p - p_j) \Big/ \prod_{\substack{j=0 \\ j\neq k}}^{n} (p_k - p) \quad j,k=0,1,2, \ldots ,n$$

Thus L_k is a polynomial of degree n. The first four terms are retained for interpolating C_p and Z values as a function of pressure. p_is are the values of pressure for which the values of specific heat and the compressibility factor have been tabulated. The pressure decrement was

taken to be one atmosphere between 100 atm and 1 atm, 0.1 atm up to 0.1 atm pressure and further reduced to 0.01 atm from then on. The lapse rate is then computed from a finite difference form of (5) with a temperature step of 10K.

The thickness of a layer corresponding to the pressure step was computed along the way through the use of the hypsometric equation:

$$\Delta Z = \frac{R\bar{T}}{g} \ln\frac{p_1}{p_2} \qquad (8)$$

a. Variation in acceleration due to gravity

The adiabatic change in temperature from a pressure of 100 atm to 10 atm is about 250K, for a temperature of 750K at 100 atm the altitude at 10 atm computed hypsometrically is approximately 28 km, and about 50 km for one atm. It is obvious then that the variation in the gravitational acceleration with altitude is about 3%. Thus the adiabatic change over a large pressure drop could be significantly in error, if variation in g is neglected. For this reason, the gravitational acceleration g was computed at every step during the upward marching calculations. The relevant factors used in arriving at the surface value of g (= 885.14 $cm \cdot sec^{-2}$) are listed in Table 1 and are based upon the most recent estimate of the ratio of the mass of Venus to the mass of the sun from Mariner 10 orbit parameters (Howard et al., 1974).

b. Computational stability

In order to check whether the accumulated error due to the finite pressure decrement was significant, the calculations were repeated for half the original step. At the end of 200 such steps (i.e. at one atmosphere level from an initial pressure of 100 atmospheres) the adiabatic change was within 0.5-1% of that arrived at by twice the step-size. Error in the computed adiabatic change in temperature is thus less than those caused by

the uncertainty in the tabulated values of compressibility and the specific heat at constant pressure. Small changes in the 10K step size used in the linear interpolation in T also did not cause any significant changes in the results.

c. Addition of nitrogen

The exact composition of the atmosphere on Venus is not yet known. All in situ measurements have been made at pressures less than 10 atmospheres, so that the well-mixedness of the lower atmosphere though generally assumed has not yet been firmly established. Nevertheless, measurements indicate that there may be up to 10% nitrogen (Avduevsky et al., 1968). The dry adiabatic lapse rate for a mixture of carbon dioxide and nitrogen for a given proportion of mass was computed in a simple calorimetric manner on the assumption that the two constituents change their temperature in an adiabatic process independent of each other. The lapse rate was computed independently for both carbon dioxide and nitrogen and the adiabatic change for the mixture for a given pressure drop was computed knowing the individual adiabatic change for each of the two and the proportion in which they are mixed. It has been tacitly assumed that the atmospheric composition on Venus is uniform throughout the atmosphere. The resultant adiabatic diagrams for 0%, 4%, 8%, 12%, 16%, and 20% nitrogen by mass are shown in Figs. 4-9 respectively. Fig. 10 depicts the variation of γ_{ad} with pressure for temperatures along adiabats.

The dry adiabats in these figures have been drawn with skew T-ln p coordinates for temperatures at 100 atm between 700K and 800K. The skew T axis is chosen as it tends to maximize the angle between the dry adiabats and the temperature profile (Hess, 1959). The required transformation is:

$$x = T(p) + 200.0 - \frac{100.0}{\ln 10.0} \ln p \qquad (9)$$

The dry adiabats on these diagrams are lines of constant potential temperature, (with 100 atm as reference pressure). For reasons mentioned earlier the potential temperature for a real atmosphere cannot be accurately specified through the Poisson equation:

$$\theta = T\left(\frac{p}{p_o}\right)^{R/C_p}$$

but must be determined by numerical integration.

3. Comparison of Measured (T,p) Profiles for the Atmosphere of Venus Against the Dry Adiabatic Diagrams

a. Upper atmosphere (above ~ 40 km)

Temperature profiles from Venera 8 in situ measurement and Mariner 10 entry signal (S-band) data are plotted on the skew T-log (p) diagrams in Figs. 4-9. The Venera 8 measurements start at an altitude of 53.7 km above surface of 0.51 $kg \cdot cm^2$ pressure (Marov et al., 1973). The S-band data from Mariner 10 was reduced assuming a 100% carbon dioxide atmosphere (Howard et al., 1974) and hence its interpretation regarding the static stability for a different atmospheric composition is not directly possible on the adiabatic diagrams.

The existence of a layer with a neutral lapse rate at about 1 atm level reported by Howard et al. (1974) is confirmed. Above this level the Mariner profile is highly stable as evidenced by the sharp increase in potential temperature (referred to 100 atm pressure). The high stability of the atmosphere above 3 atm level or about 40 km above the surface was observed in Mariner 5 profile (Fjeldbo et al., 1971) and Venera 8 measurements also.

Interpretations of the Venera 8 solar illumination and ground based observations by Lacis (1975) that most of the solar energy is deposited above 40 km for a homogeneous distribution of cloud particles with height and between 50 km and 80 km for a continuous cloud particle distribution

is consistent with the increasing stability observed in both the Venera 8 and Mariner 10 profiles.

It is of interest to note that both the Venera 7 and 8 vertical profiles of horizontal wind show a very large shear between about 38 km and 50 km above the surface and a small shear between about 18 km and 38 km. Such strong shear is possible in a stable environment and if it is of the semi-permanent nature, can be maintained only in a stably stratified atmosphere wherein the vertically adjacent layers are decoupled to atmospheric flow.

Going back to the earlier measurements of the temperature profiles, one again sees an increase in the static stability in the Venera 4 profile based on the lapse rate reported by Avduevsky et al. (1968) and the adiabatic lapse rates calculated here, after the altitude values of Venera 4 have been corrected for the wrong surface radius assumed by Avduevsky et al. (1968), [a discussion of the discrepancy is given by Ash et al., 1968, Science, (160), 985; and Eshelman et al., 1968].

b. Lower atmosphere

For the 100% carbon dioxide atmosphere the Venera 8 profile is seen to be super-adiabatic almost 37 km or about 5 atm pressure level. The S-band signal on Mariner 10 did not penetrate deeper than 40 km and thus no information about the deep atmospheric profile is available. Figs. 5-7 indicate that against the computed dry adiabatic lapse rates for 4%, 8%, and 12% nitrogen cases respectively the Venera 8 profile seems somewhat unstable. The immediate question that arises is if this could really exist on Venus or if there are problems in this method of computation of the dry adiabatic lapse rates.

If there is a significant amount of latent heat release in the lower atmosphere then the moist adiabatic lapse rate will apply. However the moist-adiabatic lapse rate is lower in magnitude than the dry adiabatic lapse rate and thus the problem of stability of the lower atmosphere worsens. Nevertheless there is not conclusive evidence for large amounts of latent heat release in the lower atmosphere of Venus and the dry adiabatic lapse rate may be assumed to apply in absnece of any evidence to the contrary.

There are three possible sources of uncertainty. The first one is the error in the in situ measurement of temperature profile and in the reduction of radio occultation data. Second, the specific heat and compressibility factors are accurate to within 1-2%, and third, the assumed atmospheric composition, either 100% carbon dioxide or 96% carbon dioxide and 4% nitrogen by mass may not be very realistic for Venus.

It should be borne in mind here that a very accurate indication of the measurement error for the temperature profiles is unavailable. The accuracy of the Mariner 5 and Mariner 10 radio occulatation measurements is limited by the fact that an atmospheric composition must be known beforehand and the sampling volume is relatively large. Note that the Mariner 10 and Venera 8 profiles do not agree well between about 3 atm and 0.7 atm. Further, the temperature at a certain level above the surface needs to be specified as an initial condition, though it does not seem to affect the derived temperature profile below about 80 km (Howard et al., 1974).

The temperature profile measurements by the Venera probes have different kinds of problems associated with them. These are all in situ measurements. The errors in the temperature profiles could be due to errors in not only the temperature sensors, but also the altimeter and pressure sensor. Ainsworth and Herman (1974) indicate the many possible interpretations of Venera 8

measurements for constructing a temperature profile.

The RMS error in Venera 8 temperature profiles is $\pm$7K (Marov et al., 1973). The difference between the surface temperature (at 92.87 $\pm$ 1.5 atm) 741 $\pm$ 7K and the 10 atm temperature (481 $\pm$ 7K) is thus 260 $\pm$ 14K. The adiabatic change in temperature for a parcel at 741K initially the surface pressure and rising to 10 atm is approximately 244K, for the 100% CO_2 case. As indicated earlier, the tabulated specific heat capacities used in the calculations are within about 1-2% of the measured values so that the uncertainty in the adiabatic change from the surface pressure value to the 10 atm level of 244K is about $\pm$5K.

The corresponding values for the 4% nitrogen and 8% nitrogen are $\sim$248 $\pm$ 5K and 252 $\pm$ 5K. Based on these uncertainties both in temperature profile and the adiabatic diagram, the possibility of a deep superadiabatic layer below 10 atm level for 70 to 12% of nitrogen in the atmosphere can not be confirmed. Essentially the same conclusion is arrived at from all previous in situ temperature measurements available.

If the available temperature profiles in the deep layers of the atmosphere of Venus are accepted at face value then in order to obtain a neutral temperature lapse rate would require greater amounts of nitrogen. If nitrogen is the only other significant constituent of the deep atmosphere as far as adiabatic processes are concerned then 16-20% of nitrogen by mass with 84-80% carbon dioxide composition yields dry adiabatic lapse rates which would make the observed temperature profiles neutral with regards to vertical displacements.

4. Summary

A detailed computation of adiabats for the Venusian atmosphere based on the known limits on its composition and the available thermodynamic data for these constituents indicate the following:

1. All available measurements of the temperature profiles for the atmosphere on Venus show a dramatic increase in the static stability between about 3 and 6 atmospheres level, depending on the amount of nitrogen (the limits are for 0% and 8% nitrogen respectively). The in situ measurements have been in the vicinity of the equator of the planet near the morning terminator, and the discussion herein pertains mostly to the tropical regions.
2. Computations indicate that there is a likelihood of a deep superadiabatic layer below a level of about 5 and 8 atmospheres, depending on the atmospheric composition. This agrees with the detection of turbulence around 1.5 to 2 atmospheres by Mariner 5, Mariner 10 and the Veneras 4 through 8 measurements.
3. Up to 20% nitrogen by mass needs to be present in the atmosphere to reduce the lower atmosphere to an adiabatic state, according to the results (see Fig. 7).

The accuracy of the adiabatic temperature changes for a given pressure change and a given composition is limited by the accuracy of the specific heat and the compressibility measurements, which for both carbon dioxide and nitrogen are about 2%. The uncertainty in adiabatic temperature changes is thus about 2%.

In order to really establish or deny the existence of superadiabatic layers on Venus, one needs more accurate knowledge of the atmospheric composition, the thermodynamic properties, and the effects of any minor condensable constituents, whose effect has been ignored in the present work. It should be useful indeed if it were possible to synthesize the Venusian atmosphere in the laboratory and to deduce the thermodynamic properties. Until then, one must wait for more accurate measurements of

the temperature profile and also the composition.

The spatial variation of the thermal field in the atmosphere of Venus is not very well known. It is possible that the vertical thermal structure in the polar regions is different from that in the equatorial regions and there may be small but significant day-night differences. It is hoped that the Pioneer Multiprobe mission to Venus and the Pioneer Orbiter mission in 1978 will yield data towards a better definition of the thermal field.

ACKNOWLEDGEMENTS

The authors thank Dr. M. J. S. Belton for his comments and interes in the present work. This research was supported by NASA Grant #NGR-50-002-189.

TABLE 1

Ratio of Mass of Sun to Mass of Venus (Howard, et.al. 1974) = 408,523.9±1.2

Equivalently, product of gravitational constant mass of sun = 324,858.6±1.0 km^3 sec^{-2}

Radius of Venus = 6053.0 km

ALTITUDE	ACCELERATION DUE TO GRAVITY
0 km	885.14 cm sec^{-2}
10	882.2
20	879.3
30	876.4
40	873.5
50	870.4
60	867.9
70	865.0
80	862.0

LIST OF FIGURES

REFERENCES

Ainsworth, J. E. and J. R. Herman, 1974: An Analysis of the Venera 8 Measurements, NASA/GSFC X- 623-74-37, Greenbelt, Maryland.

Ash, M. E., D. B. Campbell, R. B. Dyce, R. P. Ingall, R. Jurgens, G. H. Pettengill, I. I. Shapiro, M. A. Slade, T. W. Thompson, 1968: The Case for the Radar Radius of Venus. Science, (160), 985.

Avduevsky, V. S., M. Y. Marov and M. K. Rozhdestvensky, 1968: Model of The Atmosphere of the Planet Venus Based on Results of Measurements Made by the Soviet Automatic Interplanetary Station Venera 4. J. Atmos. Sci., (25), 537-545.

Avduevsky, V. S., M. Y. Marov, and M. K. Rozhdestvensky, 1970: Preliminary Results of Measurements by Space Probes Venera 5 and Venera 6 in the Atmosphere of Venus. Radio Sci., (5), 333-338.

Avduevsky, V. S., M. Y. Marov, and M. K. Rozhdestvensky, N. F. Borodin, and V. V. Kerzanovich, 1971: Landing of the Automatic Station Venera 7 on the Venus Surface and Preliminary Results of Investigations of the Venus Atmosphere. J. Atmos. Sci., (28), 263-269.

Conte, S. D., 1965: Elementary Numerical Analysis, McGraw Hill Book Company, New York. 278 pp.

Eshelman, V. R.,G. Fjeldbo, J. D. Anderson, A. Kliore, R. B. Dyce, 1968: Venus: Lower Atmospheres Not Measured. Science, (162), 661-665.

Fjeldbo, G. and A. J. Kliore, and V. R. Eshelman, 1971: The Neutral Atmosphere of Venus as Studied with the Mariner 5 Radio Occultation Experiments. Astron. J. (76), 123-140.

Hess, S. L., 1959: Introduction to Theoretical Meteorology. Holt, Rinehart, and Winston, New York. 362 pp.

Hilsenrath, J., C. W. Becket, W. S. Benedict, L. Farro, H. J. Hoge, J. F. Masi, R. L. Nuttal, Y. S. Toulobian, and H. W. Woolley, 1960: Tables of Thermodynamic and Transport Properties of Air, Argon, Carbon Dioxide, Carbon Monoxide, Hydrogen, Nitrogen, Oxygen and Steam. Pergamon Press, New York.

Howard, H. T., G. L. Tyler, G. Fjeldbo, A. J. Kliore, G. S. Levy, D. L. Brunn, R. Dickinson, R. E. Edelson, W. L. Martin, R. B. Postal, B. Seidel, T. T. Sesplauleis, D. L. Shirley, C. T. Stelzried, D. N. Sweetnam, Z. I. Zygielbaum, P. B. Esposito, J. D. Anderson, I. I. Shapiro, and R. D. Reasenberg, 1974: Venus: Mass, Gravity Field, Atmosphere, and Ionosphere as Measured by the Mariner 10 Dual Frequency Radio System. Science, (183), 1297-1306.

Lacis, 1974: Paper presented at the Conference on the Atmosphere of Venus, Goddard Institute of Space Studies, New York, 15-17 October 1974. [Also NASA Publication SP-382 (1975)]

Marov, M. Y., V. S. Avduevsky, V. V. Kerzhanovich, M. K. Rozhdestvensky, N. F. Borodin, and O. L. Ryabou, 1973: Venera 8 Measurements of Temperature, Pressure, and Wind Velocity on the Illuminated Side of Venus. J. Atmos. Sci. (30), 1210-1214.

Marov, M. Y., 1972: A Perspective in the Beginning of Planetary Exploration, Icarus, (16), 415-461.

Staley, D. O., 1970: The Adiabatic Lapse Rate in the Venus Atmosphere, J. Atmos. Sci., (27), 219-223.

Vinogradov, A. P., Yu. A. Surkov, and C. P. Florensky, 1968: The Chemical Composition of the Venus Atmosphere Based on the Data of the Interplanetary Station Venera 4, J. Atmos. Sci., (25), 535-536.

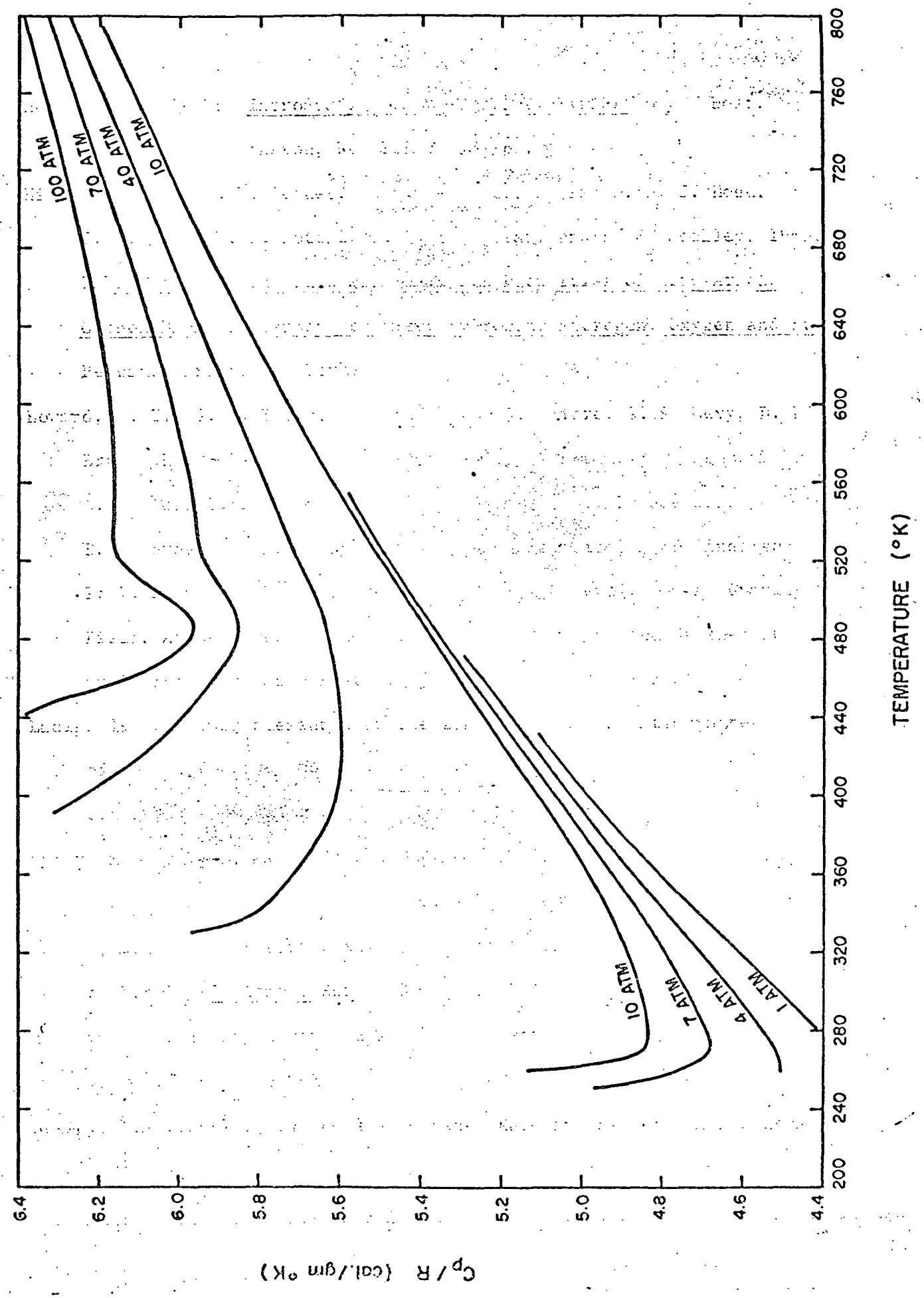
100 ATM
70 ATM
40 ATM
10 ATM
10 ATM
7 ATM
4 ATM
1 ATM
6.4
6.2
6.0
5.8
5.6
5.4
5.2
5.0
4.8
4.6
4.4
200
240
280
320
360
400
440
480
520
560
600
640
680
720
760
800
TEMPERATURE (°K)
C_p / R (cal./gm °K)

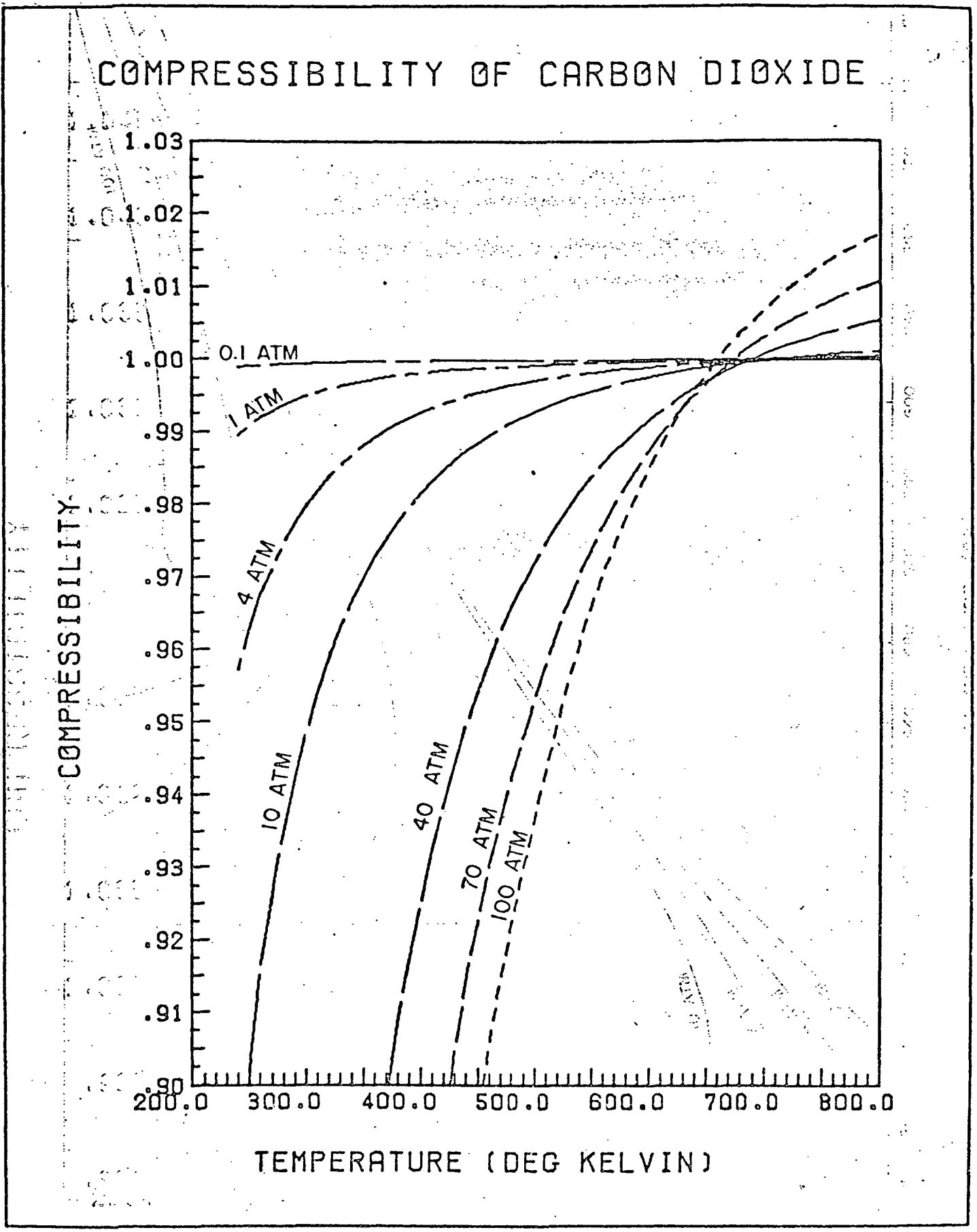
COMPRESSIBILITY OF CARBON DIOXIDE
COMPRESSIBILITY
1.03
1.02
1.01
1.00
.99
.98
.97
.96
.95
.94
.93
.92
.91
.90
0.1 ATM
1 ATM
4 ATM
10 ATM
40 ATM
70 ATM
100 ATM
200.0
300.0
400.0
500.0
600.0
700.0
800.0
TEMPERATURE (DEG KELVIN)

COMPRESSIBILITY OF NITROGEN

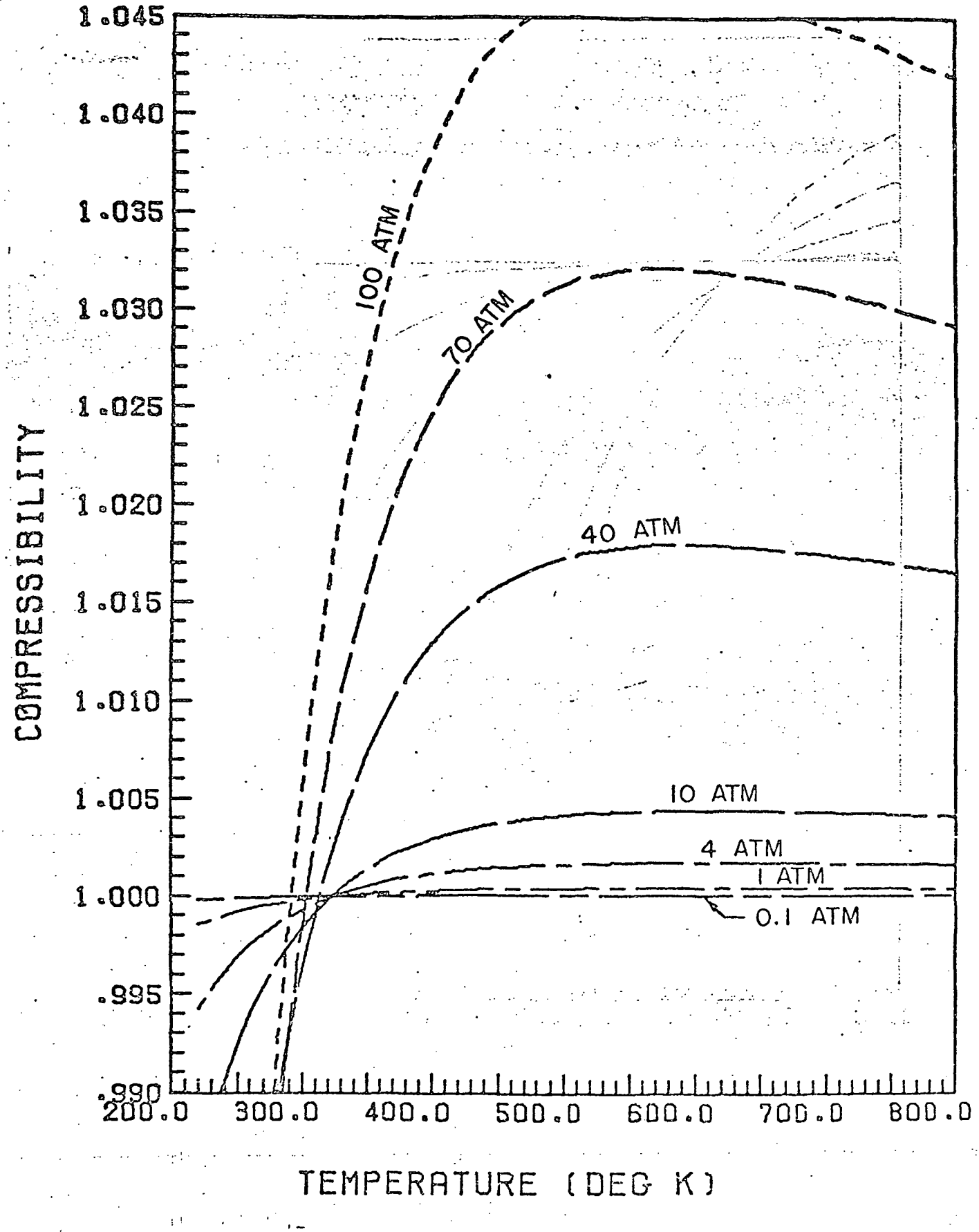

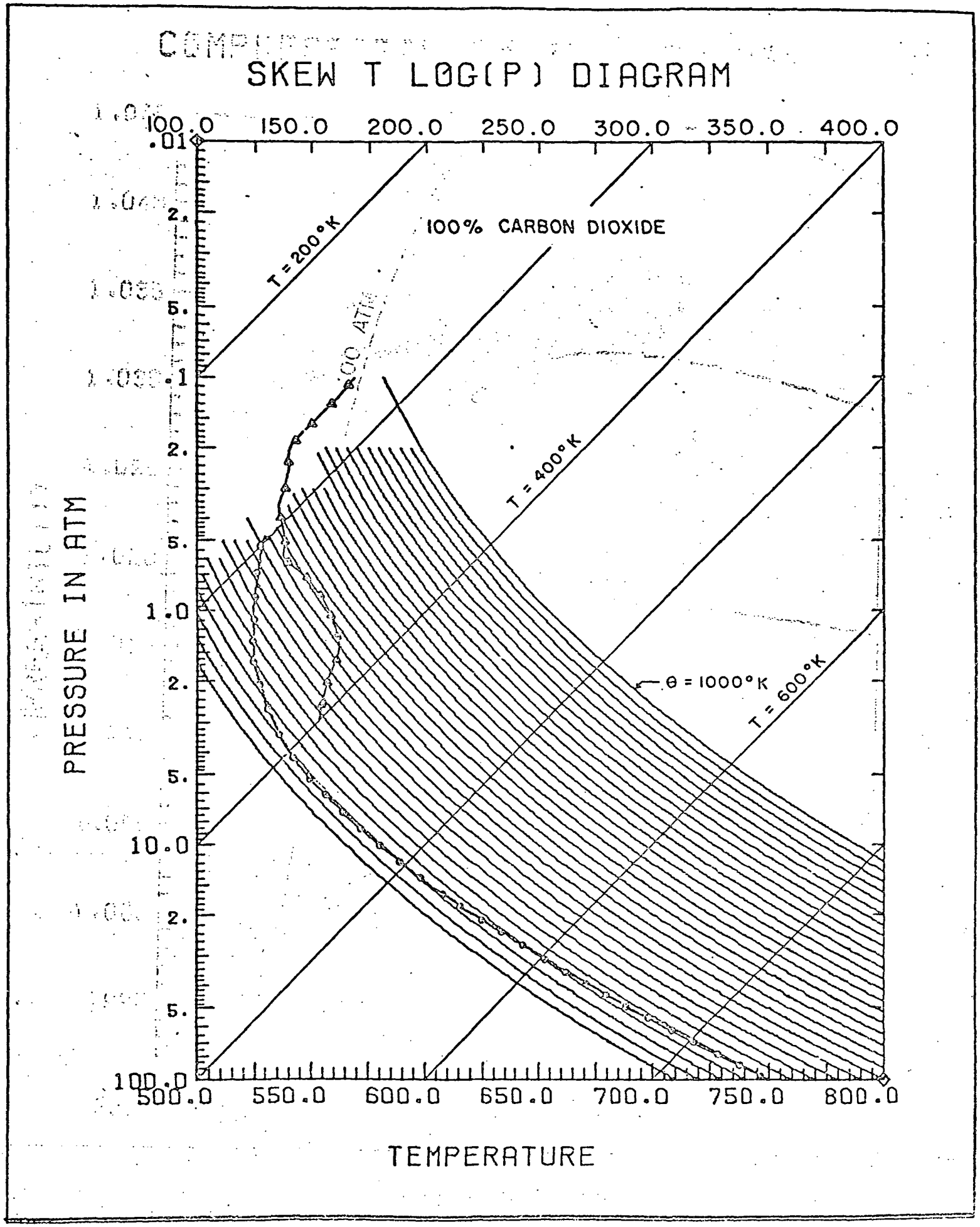
SKEW T LOG(P) DIAGRAM
100.0
150.0
200.0
250.0
300.0
350.0
400.0
.01
2.
5.
.1
2.
5.
1.0
2.
5.
10.0
2.
5.
100.0
500.0
550.0
600.0
650.0
700.0
750.0
800.0
T=200°K
100% CARBON DIOXIDE
100 ATM
T=400°K
θ=1000°K
T=600°K
PRESSURE IN ATM
TEMPERATURE

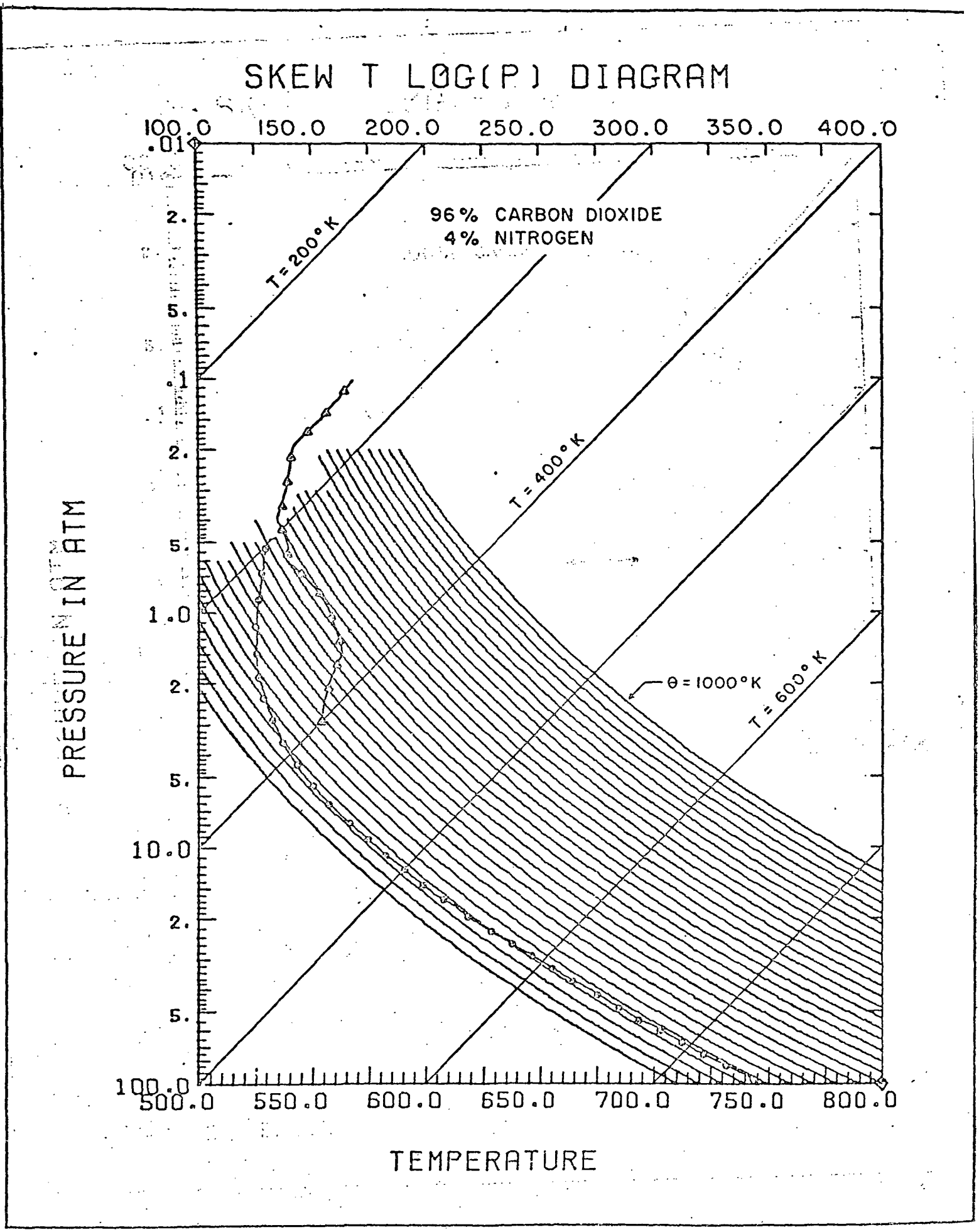
SKEW T LOG(P) DIAGRAM
100.0
150.0
200.0
250.0
300.0
350.0
400.0
.01
2.
5.
.1
2.
5.
1.0
2.
5.
10.0
2.
5.
100.0
96% CARBON DIOXIDE
4% NITROGEN
T=200°K
T=400°K
T=600°K
θ=1000°K
PRESSURE IN ATM
500.0
550.0
600.0
650.0
700.0
750.0
800.0
TEMPERATURE

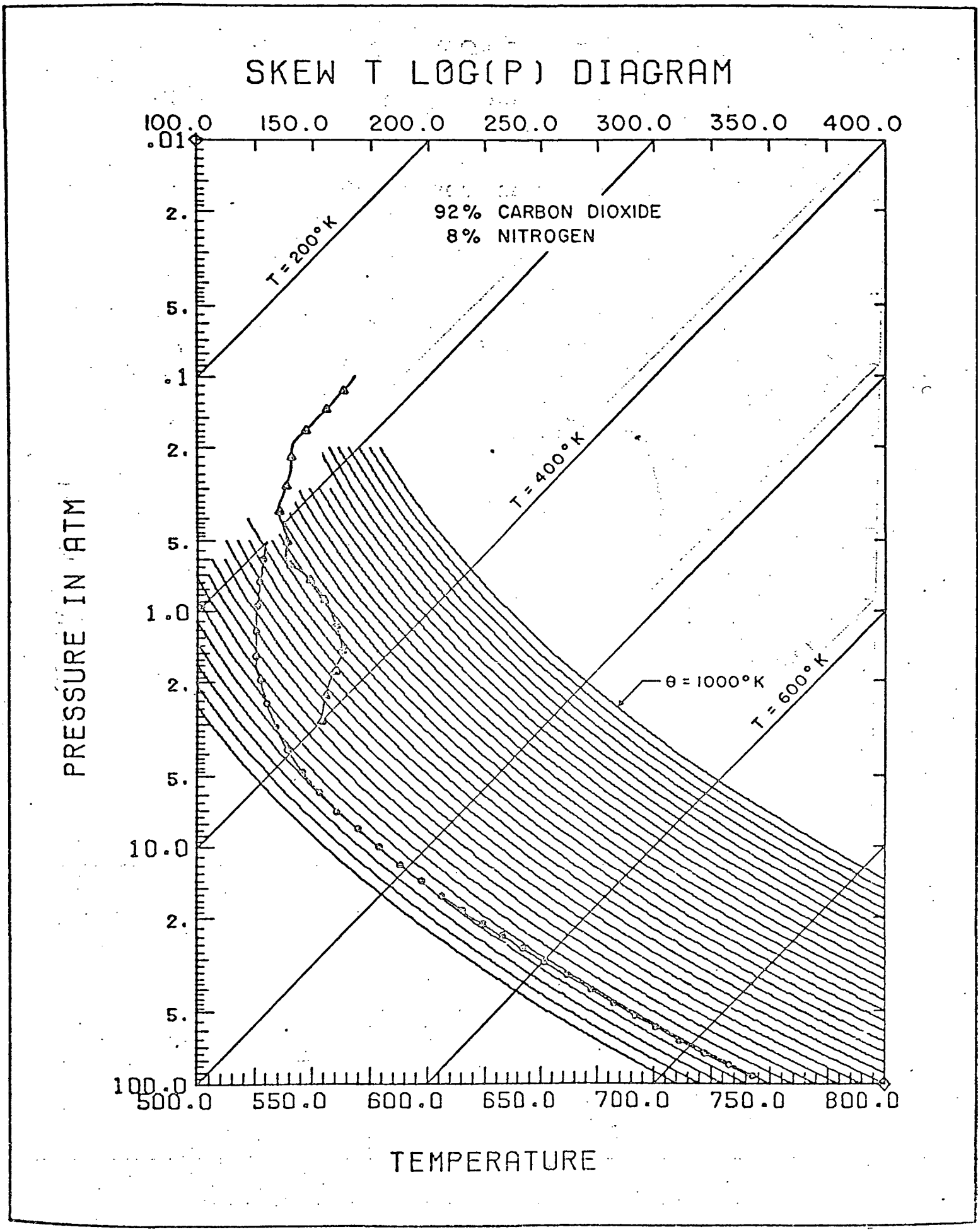
SKEW T LOG(P) DIAGRAM
100.0
150.0
200.0
250.0
300.0
350.0
400.0
.01
2.
5.
.1
2.
5.
1.0
2.
5.
10.0
2.
5.
100.0
500.0
550.0
600.0
650.0
700.0
750.0
800.0
92% CARBON DIOXIDE
8% NITROGEN
T = 200°K
T = 400°K
T = 600°K
θ = 1000°K
PRESSURE IN ATM
TEMPERATURE

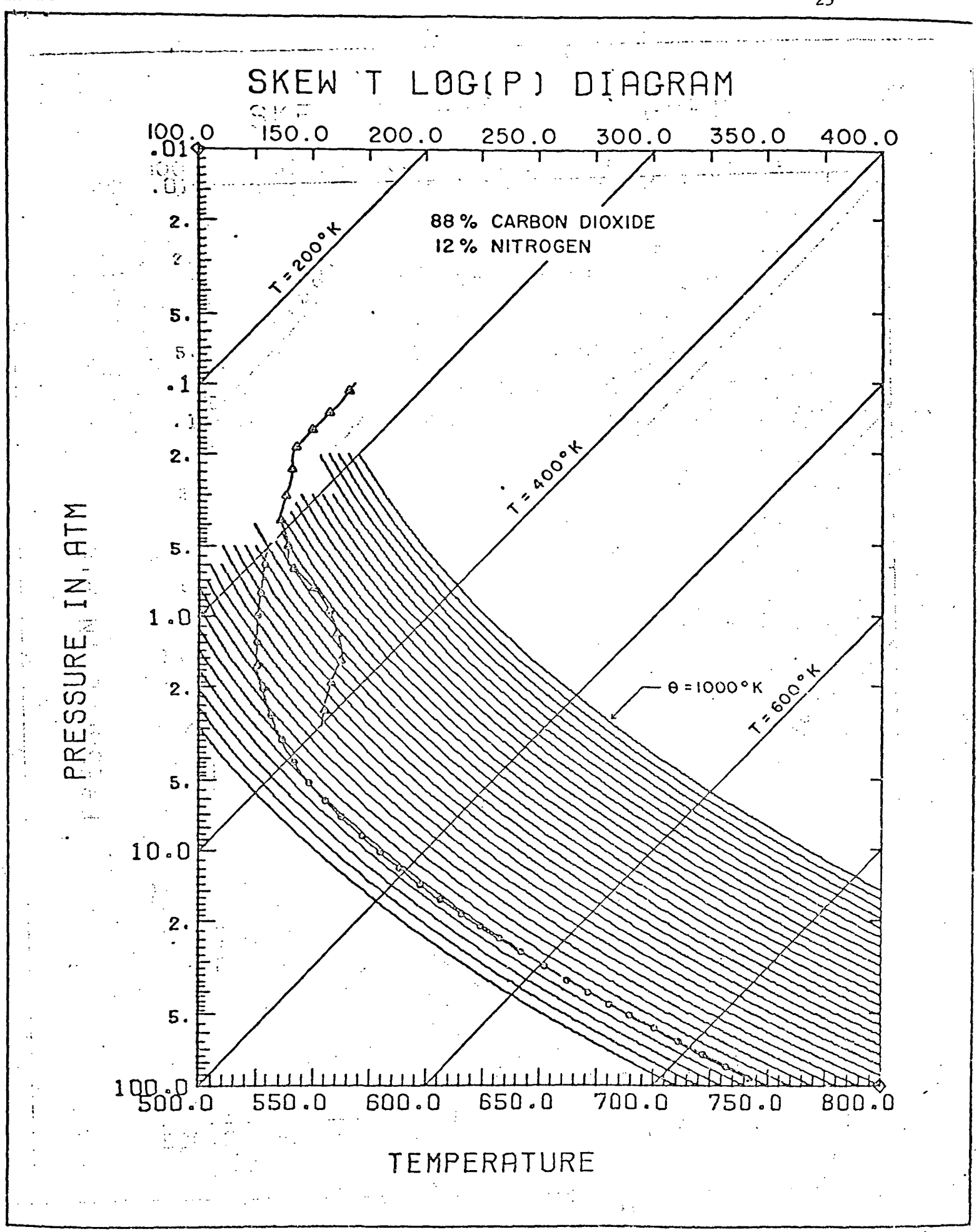
SKEW T LOG(P) DIAGRAM
100.0
150.0
200.0
250.0
300.0
350.0
400.0
.01
.02
.05
.1
.2
.5
1.0
2.
5.
10.0
20.
50.
100.0
88% CARBON DIOXIDE
12% NITROGEN
T=200°K
T=400°K
T=600°K
θ=1000°K
PRESSURE IN ATM
500.0
550.0
600.0
650.0
700.0
750.0
800.0
TEMPERATURE

SKEW T LOG(P) DIAGRAM

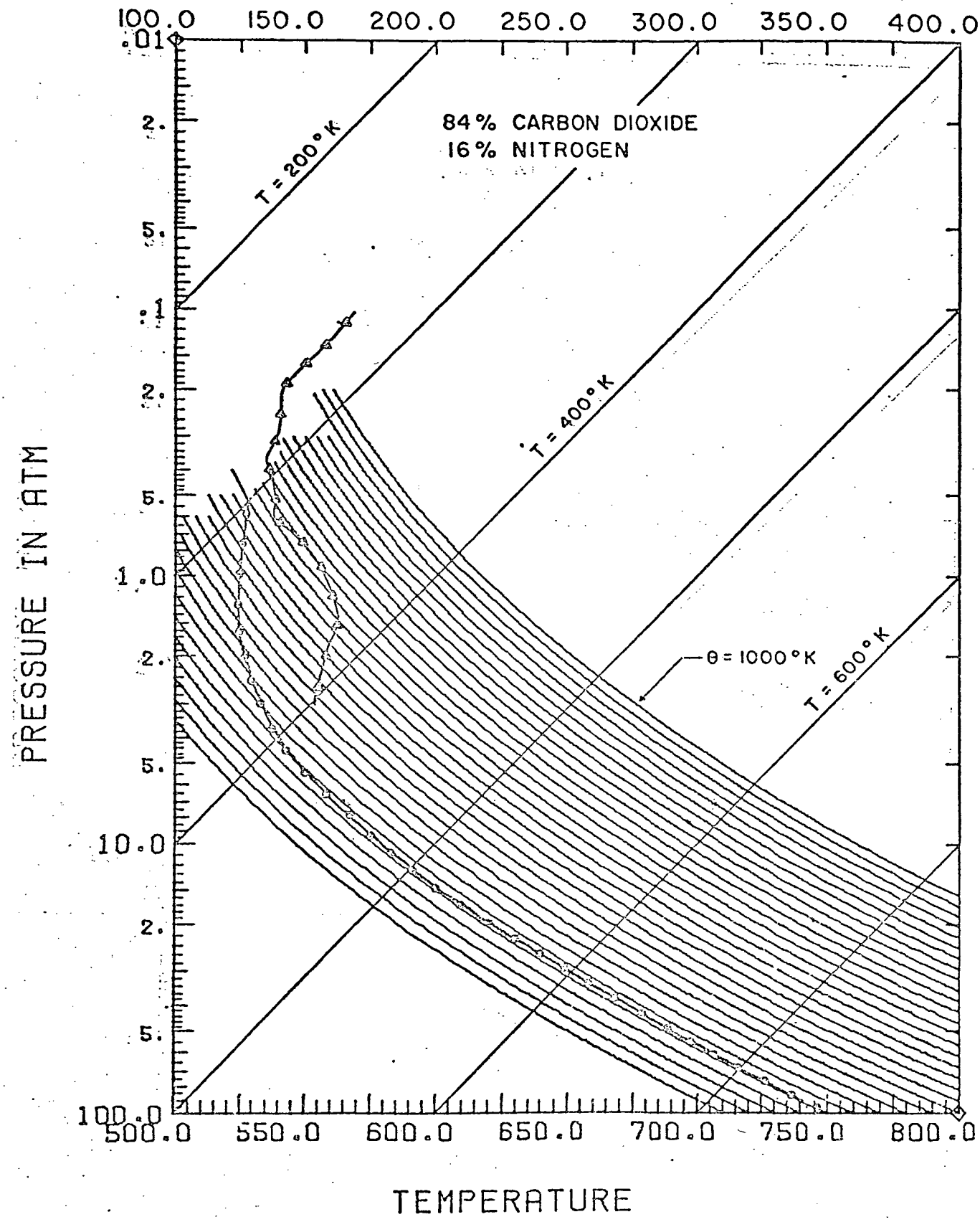

SKEW T LOG(P) DIAGRAM

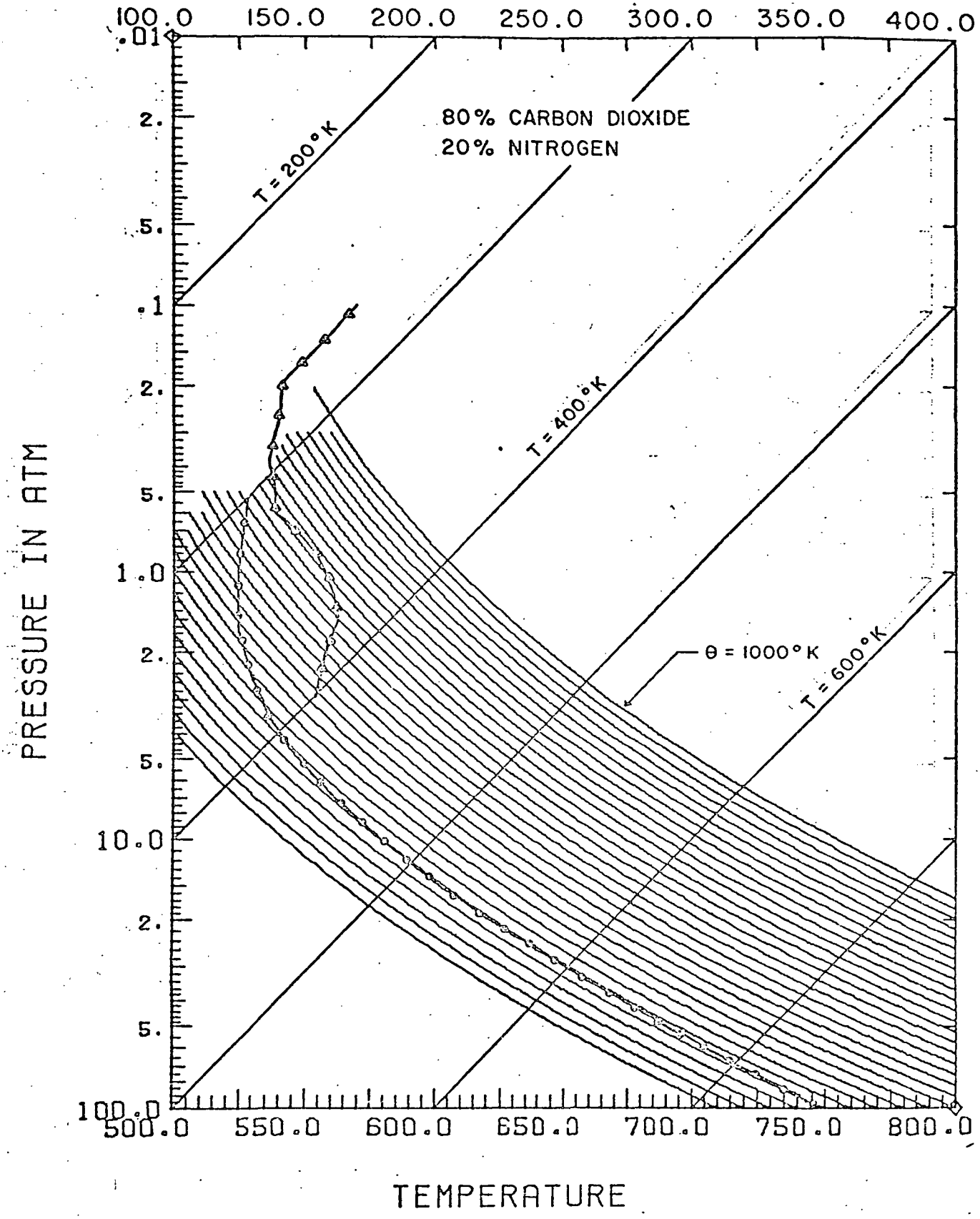

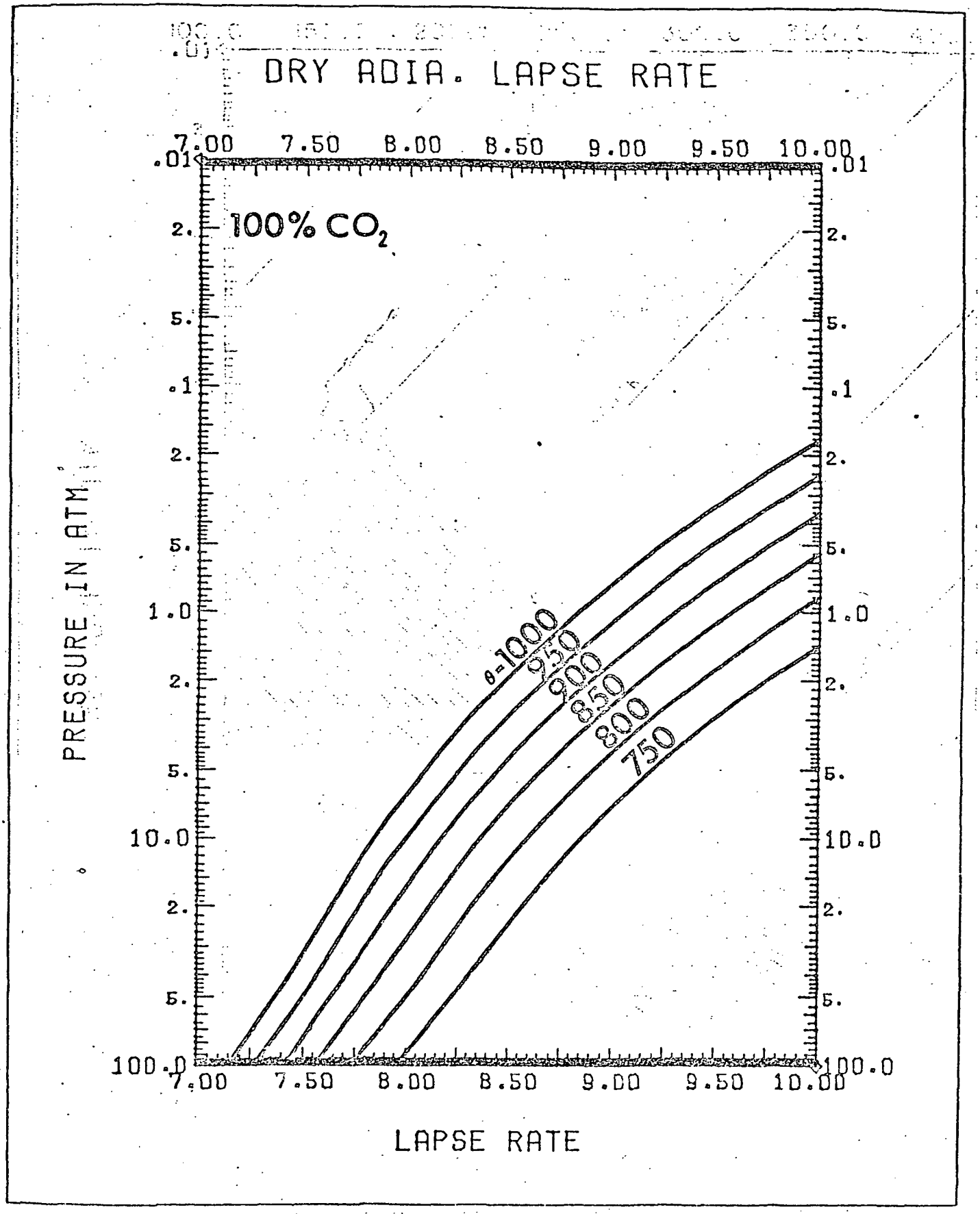
DRY ADIA. LAPSE RATE
100% CO_2
θ=1000
950
900
850
800
750
PRESSURE IN ATM
LAPSE RATE
7.00
7.50
8.00
8.50
9.00
9.50
10.00
.01
2.
5.
.1
1.0
10.0
100.0